



1

2 **A Unified Framework for Surface Flux-Driven Cyclones Outside the Tropics**

3 Kerry Emanuel (1), Tommaso Alberty (2), Stella Bourdin (3), Suzana J. Camargo (4), Davide
 4 Faranda (5,6,7), Manos Flaounas (8,9), Juan Jesus Gonzalez-Aleman (10), Chia-Ying Lee (4),
 5 Mario Marcello Miglietta (11), Claudia Pasquero (12), Alice Portal (13), Hamish Ramsay (14),
 6 Romualdo Romero (15)

7 (1) Massachusetts Institute of Technology, 77 Mass. Ave., Cambridge, MA 02139

8 (2) Istituto Nazionale di Geofisica e Vulcanologia, Rome, Italy

9 (3) Atmospheric, Oceanic and Planetary Physics, Department of Physics, University of Oxford,
 10 Oxford, United Kingdom

11 (4) Lamont-Doherty Earth Observatory, Columbia University, Palisades, New York, USA

12 (5) Laboratoire des Sciences du Climat et de l'Environnement, UMR 8212 CEA-CNRS-UVSQ,
 13 Université Paris-Saclay & IPSL, CE Saclay l'Orme des Merisiers, 91191 Gif-sur-Yvette,
 14 France

15 (6) London Mathematical Laboratory, 8 Margravine Gardens, London W6 8RH, UK

16 (7) LMD/IPSL, ENS, Université PSL, École Polytechnique, Institut Polytechnique de Paris,
 17 Sorbonne Université, CNRS, Paris France

18 (8) Institute for Atmospheric and Climate Science, ETH Zurich, Zurich, Switzerland

19 (9) Institute of Oceanography, Hellenic Centre for Marine Research, Athens, Greece

20 (10) CNR-ISAC, Padua, Italy

21 (11) Spanish State Meteorological Agency, AEMET, Department Development and Applications

22 (12) Department of Earth and Environmental Sciences, University of Milano - Bicocca, Italy

23 (13) Institute of Atmospheric Sciences and Climate (CNR-ISAC), National Research Council of
 24 Italy, Bologna, Italy

25 (14) CSIRO Environment, Aspendale, Victoria, Australia

26 (15) Grup de Meteorologia, Departament de Física, Universitat de les Illes Balears, Palma de
 27 Mallorca, Spain

28 Correspondence: Kerry Emanuel (emanuel@mit.edu)



29

30

Abstract

31 Cyclonic storms resembling tropical cyclones are sometimes observed well outside the tropics.
 32 These include medicanes, polar lows, subtropical cyclones, Kona storms, and possibly some
 33 cases of Australian East Coast cyclones. Their structural similarity to tropical cyclones lies in
 34 their tight, nearly axisymmetric inner cores, eyes, and spiral bands. Previous studies of these
 35 phenomena suggest that they are partly and sometimes wholly driven by surface enthalpy
 36 fluxes, as with tropical cyclones. Here we show, through a series of case studies, that many of
 37 these non-tropical cyclones have morphologies and structures that resemble each other and
 38 also closely match those of tropical transitioning cyclones, with the important distinction that the
 39 potential intensity that supports them is not present in the pre-storm environment but rather is
 40 locally generated in the course of their development. We therefore propose to call these storms
 41 CYCLOnes from Locally Originating Potential intensity (CYCLOPs). Like their tropical cousins,
 42 the rapid development and strong winds of cyclops pose a significant threat and forecast
 43 challenge for islands and coastal regions.

44 1. Introduction

45 Cyclones that resemble tropical cyclones are occasionally observed to develop well outside the
 46 tropics. These include polar lows, medicanes, subtropical cyclones, Kona storms (central North
 47 Pacific), and perhaps some cases of Australian East Coast cyclones. The identification of such
 48 systems is usually based on their appearance in satellite imagery and on the environmental
 49 conditions in which they occur. Here we show that many of these systems are manifestations of
 50 the same physical phenomenon and, as such, should be given a common, physically-based
 51 designation. We propose to call these CYCLOnes from Locally Originating Potential intensity
 52 (CYCLOPs), with reference to the single-eyed creatures of Greek mythology¹. We show that in
 53 many respects these developments resemble classical “tropical transition” (TT) events (e.g.
 54 Bosart and Bartlo, 1991), but they are distinguished from the latter by occurring in regions
 55 where the climatological potential intensity is small or zero. Their rapid development and intense
 56 mesoscale inner cores, compared to extratropical cyclones, make cyclops significant hazards
 57 and a forecasting challenge.

58 Cyclones of synoptic and sub-synoptic scale are powered by one or both of two energy sources:
 59 the available potential energy (APE) associated with isobaric temperature gradients
 60 (baroclinity), and fluxes of enthalpy (sensible and latent heat) from the ocean to the

¹ Late in the process of writing this paper, we discovered that there is a scientific research project by the same name, standing for “Improving Mediterranean CYCLOnes Predictions in Seasonal forecasts with artificial intelligence” (<https://www.cmcc.it/projects/cyclops-improving-mediterranean-cyclones-predictions-in-seasonal-forecasts-with-artificial-intelligence>). Its team leader, Leone Cavicchia, has graciously agreed with our use of the same name.



61 atmosphere². A normal extratropical cyclone over land is an example of the former, while the
 62 latter is epitomized by a classical tropical cyclone. Extratropical transitioning and tropical
 63 transitioning cyclones³ are powered by both sources, with the relative proportion usually varying
 64 over the life of the storm. Additionally, we note that tropical cyclones often originate in
 65 disturbances, such as African easterly waves, that derive their energy from isobaric temperature
 66 gradients.

67 Like tropical cyclones, cyclops are mainly powered by surface enthalpy fluxes, but differ from
 68 the former in that the required potential intensity is produced locally and transiently by baroclinic
 69 processes, whereas tropical cyclones develop in seasons and regions where potential intensity
 70 is always present. Cyclops closely resemble the strongly baroclinic cases of tropical transition
 71 defined and discussed by Davis and Bosart (2004), except that they occur in regions where the
 72 climatological potential intensity is too small for tropical cyclogenesis, relying on synoptic-scale
 73 perturbations that locally enhance potential intensity in space and time. David and Bosart (2004)
 74 confined their attention to tropical cyclone formation in regions of high sea surface temperature,
 75 stating that “The precursor cyclone must occlude and remain over warm water ($\geq 26^\circ\text{C}$) for at
 76 least a day following occlusion.” Similarly, McTaggart-Cowan et al. (2008) and McTaggart-
 77 Cowan et al. (2013) only examined cases of tropical transition that resulted in named tropical
 78 cyclones. But McTaggart-Cowan et al. (2015) recognized that around 5% of the cases they
 79 identified as tropical transition cases occurred over colder water and that upper-level troughs
 80 played a key role in destabilizing the atmosphere with respect to the sea surface. We here build
 81 on this work and place it within the framework of potential intensity theory.

82 The basic physics of cyclops was explored by the first author in reference to medicanes, and is
 83 illustrated in Figure 1. While the actual evolution is, of course, continuous, it is simpler to
 84 discuss it in phases. In the first phase (Figure 1a), Rossby wave breaking has resulted in an
 85 isolated potential vorticity (PV) anomaly near the tropopause. We idealize this anomaly as
 86 circularly symmetric and show a cross-section through it. In the illustration, the first phase is
 87 assumed to occur over land, but that need not be the case in general.

² Some would regard latent heating as an additional energy source, but condensation through a deep layer is present in most cyclones and, being strongly tied to vertical motion, should not be regarded as an external heat source but rather as a modification of the effective static stability.

³ Extratropical transitioning cyclones are storms whose energy source is transitioning from surface fluxes to ambient baroclinity, while the energy source of tropical transitioning cyclones is moving in the opposite direction.

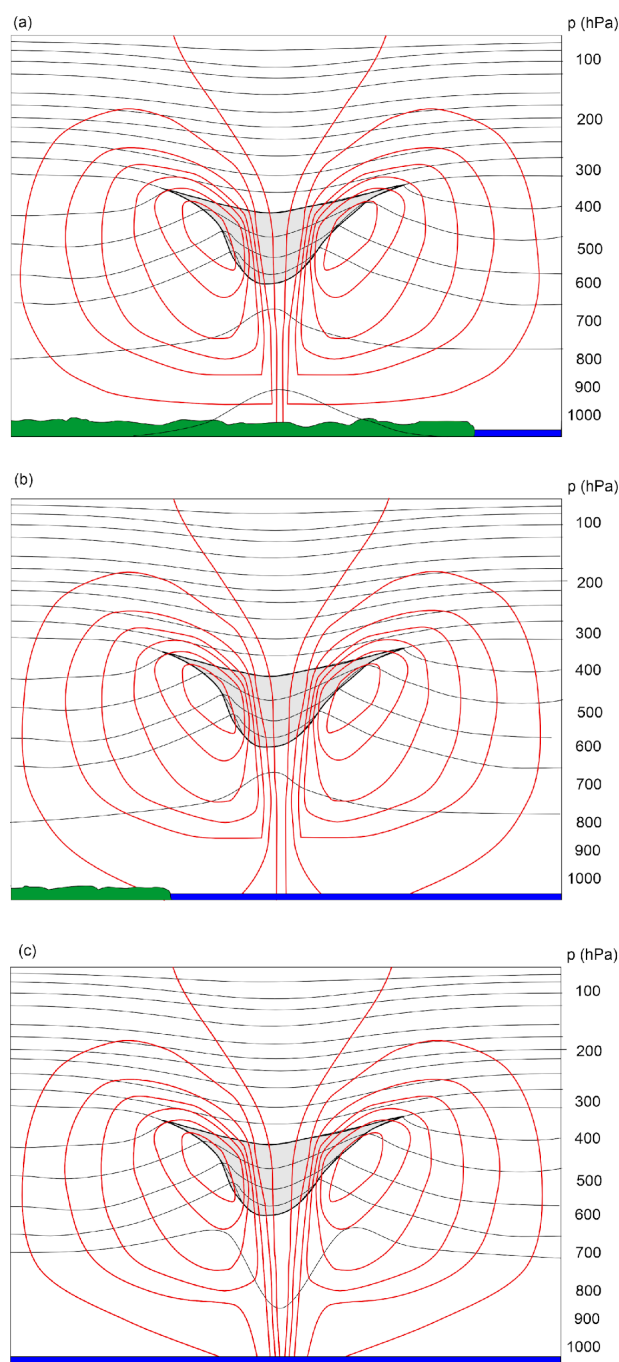


Figure 1: Three stages in the development of a cyclop. Each of the three panels shows a cross-section through a circular, isolated PV anomaly at the tropopause (gray shading). The thin black curves are isentropes, while the red curves are isotachs of the flow normal to the cross-section. In the first phase (a), the PV anomaly is over land, the troposphere beneath it is anomalously cold, and there may be no flow at the surface. The system moves out over open water in the next phase (b) and warming of the boundary layer and lower troposphere suffices to eliminate the cold anomaly at and near the surface. Weak cyclonic flow develops in response to the positive PV anomaly aloft. In the final phase (c), the surface heat fluxes become important and a tight, inner warm core develops.



89 During the creation of the near-tropopause PV anomaly, some combination of lifting and cold air
90 seclusion has cooled and moistened the column underneath the PV anomaly, and the cold
91 anomaly extends right to the surface. From a PV inversion perspective, the near-surface
92 anticyclone that results from inverting the negative potential temperature anomaly at the surface
93 is assumed to just cancel the cyclonic anomaly that results from inverting the tropopause PV
94 anomaly, yielding no circulation at the surface.

95 In phase 2 (Figure 1b), the system drifts out over open water that is warm enough to diminish
96 and eventually eliminate the cold anomaly at the surface, “unshielding” it from the PV anomaly
97 aloft. During this phase, a cyclonic circulation develops in the lower troposphere, with a
98 horizontal scale commensurate with that of the PV anomaly.

99 If the local potential intensity is large enough, and the air aloft sufficiently close to saturation,
100 Wind-Induced Surface Heat Exchange (WISHE) can develop a tropical cyclone-like vortex
101 (phase3, Figure 1c), with a warm inner core, eye and eyewall, and perhaps spiral bands. Note
102 that the inner core may be warm only with respect to the synoptic-scale cold anomaly
103 surrounding it, not necessarily with respect to the distant environment. At mid-levels, the
104 temperature anomaly may manifest as a small-scale warm anomaly surrounded by a synoptic-
105 scale cold anomaly.

106 In reality, these phases blend together into a continuum. One practical challenge is calculating
107 the potential intensity. This should be calculated using the temperatures of the sea surface and
108 the free troposphere under the PV anomaly aloft, but before the troposphere has appreciably
109 warmed from surface fluxes. In practice, because the warming occurs either as the PV anomaly
110 develops over water, or as it moves over water from land, we have no access to the sounding of
111 the free troposphere *before* it has warmed up. The true potential intensity for a TC developing
112 within the cold column under the PV anomaly is hence impossible to obtain. Nevertheless, we
113 can estimate how cold the troposphere was before surface fluxes warmed it by assuming that
114 the troposphere has an approximately moist adiabatic temperature profile and using the upper
115 tropospheric geopotential height in the cold cutoff cyclone to estimate the negative temperature
116 perturbation underneath it. This was done in Emanuel (2005) and a slightly improved version is
117 derived in the Appendix. The result is a modified potential intensity, V_{pm} , given by

$$118 \quad V_{pm}^2 = V_p^2 - \frac{C_k}{C_D} \frac{T_s}{T_{400}} \phi'_{400}, \quad (1)$$

119 where V_p is the potential intensity calculated in the usual way from the local sea surface
120 temperature and atmospheric sounding, ϕ'_{400} is the perturbation of the upper tropospheric
121 geopotential, which we here evaluate at 400 hPa, away from climatology, C_k and C_D are the
122 surface exchange coefficients for enthalpy and drag, and T_s and T_{400} are the absolute
123 temperatures at the surface and 400 hPa. In what follows, we approximate the coefficient



124 multiplying ϕ'_{400} in (1) by a constant value, 1.3, a reasonable estimate of the mean value of the
 125 coefficient.

126 Beginning with an upper cold cyclone in an environment of otherwise zero potential intensity,
 127 Emanuel (2005) simulated the development of a WISHE-driven cyclone using the axisymmetric,
 128 nonhydrostatic hurricane model of Rotunno and Emanuel (1987). The cold, moist troposphere
 129 under such an upper cyclone proves to be an ideal incubator of surface flux-driven cyclones
 130 with characteristics nearly identical to those of tropical cyclones. One interesting facet of the
 131 process is that the anomalous surface enthalpy flux destroys the parent upper cold low over a
 132 period of a few days.

133 2. Why it matters

134 Why should we care whether a cyclone is driven by surface fluxes or baroclinity? From a
 135 practical forecasting standpoint, the spatial distributions of weather hazards, like rain and wind,
 136 can be very different, as can be the development time scales and fundamental predictability.

137 In classical baroclinic cyclones, the strongest winds are often found in frontal zones and can be
 138 far from the cyclone center, and precipitation is usually heaviest in these frontal zones and in a
 139 shield of slantwise ascent extending poleward from the surface cyclone. There is long
 140 experience in forecasting baroclinic storms, and today's numerical weather prediction (NWP) of
 141 these events has become quite accurate, even many days ahead. Importantly, baroclinic
 142 cyclones are well resolved by today's NWP models. While baroclinic cyclones can intensify
 143 rapidly, both the magnitude and timing of intensification are usually forecast accurately, and
 144 uncertainties are well quantified by NWP ensembles.

145 By contrast, the physics of tropical cyclone intensification, involving a positive feedback between
 146 surface winds and surface enthalpy fluxes, results in an intense, concentrated core with high
 147 winds and heavy precipitation (which can be snow in the case of polar lows). The eyewalls of
 148 surface flux-driven cyclones are strongly frontogenetical, further concentrating wind and rain in
 149 an annulus of mesoscale dimensions. The intensity of surface flux-driven cyclones can change
 150 very rapidly and often unpredictably, presenting a severe challenge to forecasters. For example,
 151 Hurricane Otis of 2023 intensified from a tropical storm to a Category 5 hurricane in about 30
 152 hours, devastating Acapulco, Mexico, with little warning from forecasters. The small size of the
 153 core of high winds and heavy precipitation means that small errors in the forecast position of the
 154 center of the storm can lead to large errors in local wind and precipitation predictions. Surface
 155 flux-driven cyclones are too small to be well resolved by today's global NWP models, and even
 156 if they were well resolved, fundamental predictability studies show high levels of intrinsic
 157 unpredictability of rapid intensity changes (Zhang et al., 2014).

158 The time and space scales of surface flux-driven cyclones are such that they couple strongly
 159 with the ocean, producing near-inertial currents whose shear-driven turbulence mixes to the
 160 surface generally (but not always) colder water from below the surface mixed layer. This has an
 161 important (usually negative) feedback on the intensification of such cyclones. Accurate
 162 numerical forecasting of surface flux-driven cyclones therefore requires an interactive ocean,



163 generally missing from today's NWP models because it is not very important for baroclinic
 164 cyclones and because of the additional computational burden.

165 For these reasons, it matters (or should matter) to forecasters whether a particular development
 166 is primarily driven by surface fluxes or by ambient baroclinity. The structural differences
 167 described above are often detectable in satellite imagery; at the same time, such imagery is
 168 sometimes misleading about the underlying physics. For example, classical baroclinic
 169 development sometimes develops cloud-free eyes surrounded by convection through the warm
 170 seclusion process, even over land, and yet may not have the intense annular concentration of
 171 wind and rain characteristic of surface flux-driven cyclones (Tous and Romero, 2013).

172 Armed with the conceptual cyclop model developed in section 1 and modified potential intensity
 173 given by (1), we now turn to case studies of the development of medicanes, polar lows, a
 174 subtropical cyclone, and a Kona storm, showing that the dynamic and thermodynamic pathways
 175 are similar. Specifically, each case developed after the formation of a deep, cold-core cut-off
 176 cyclone in the upper troposphere that often resulted from a Rossby wave breaking event. The
 177 lifting of the tropospheric air in response to the developing potential vorticity anomaly near the
 178 tropopause created a deep, cold, and presumably humid column. The deep cold air over bodies
 179 of relatively warmer water substantially elevates potential intensity, while its high relative
 180 humidity discourages evaporatively driven convective downdrafts, which tamp down the needed
 181 increase in boundary layer enthalpy. Low vertical wind shear near the core of the cutoff cyclone,
 182 coupled with high potential intensity and humidity, provide an ideal embryo for tropical cyclone-
 183 like development.

184 In what follows we focus on the cutoff cyclone evolution and the development of modified
 185 potential intensity. In a particular case, we compare reanalysis column water vapor to that
 186 estimated from satellite measurements. The differences between these are significant enough
 187 to cast some doubt on the quality of reanalyzed water vapor associated with the small-scale
 188 cyclop developments, thus we do not focus on water vapor even though it is known to be
 189 important for intensification of tropical cyclones.

190 We also examined, but do not show here, several cases of Australian East Coast Lows (Holland
 191 et al., 1987). Owing to the East Australian Current, the climatological potential intensity is
 192 substantial off the southeast coast of Australia, and the cyclop developments we analyzed
 193 behaved more like classical tropical transitions, with little or no role of the synoptic scale
 194 dynamics in enhancing the existing potential intensity. We suspect that there may be other
 195 cases in which the latter process was important, but did not conduct a search for such cases. It
 196 is clear that in many of these cases surface heat fluxes were important in driving the cyclone
 197 (Cavichia et al., 2019). We also examined a small number of subtropical cyclones that
 198 developed in the South Atlantic, but as with the Australian cases, they resembled classical
 199 tropical transitions, though again we suspect there may be cyclop cases there as well.

200 As with tropical cyclones, there are variations on the theme of cyclops, and we explore these in
 201 the closing sections.

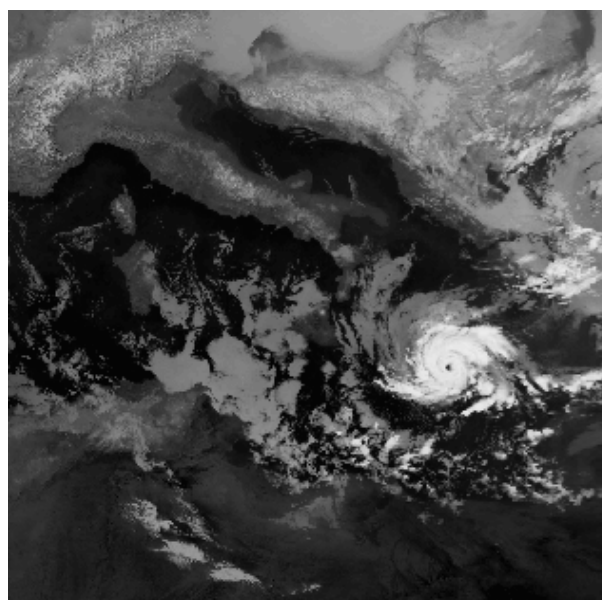
202



203 3. Case Studies

204 3.1 Mediane Celano of January, 1995

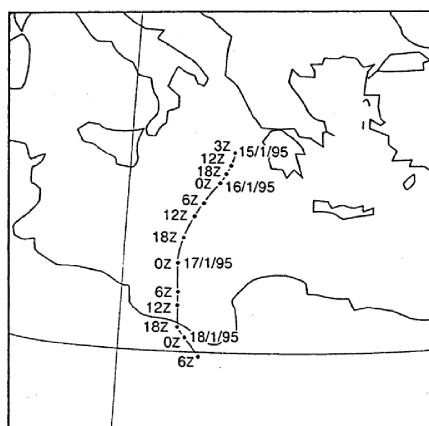
205 On average, 1.5 medicanes are observed annually in the Mediterranean (Cavicchia et al., 2014;
206 Nastos et al., 2018; Romero and Emanuel, 2013; Zhang et al., 2021) and, more rarely, similar
207 storms are observed over the Black Sea (Yarovaya et al., 2008). We begin with a system,
208 Mediane Celano, that reached maturity on 16 January, 1995, shown in infrared satellite
209 imagery in Figure 2.



210

211 *Figure 2: Infrared satellite image of Mediane Celano in the central Mediterranean, at 09:06 UTC 16 January 1995.*
212 *(Image credit: NOAA, 1995)*

213



214

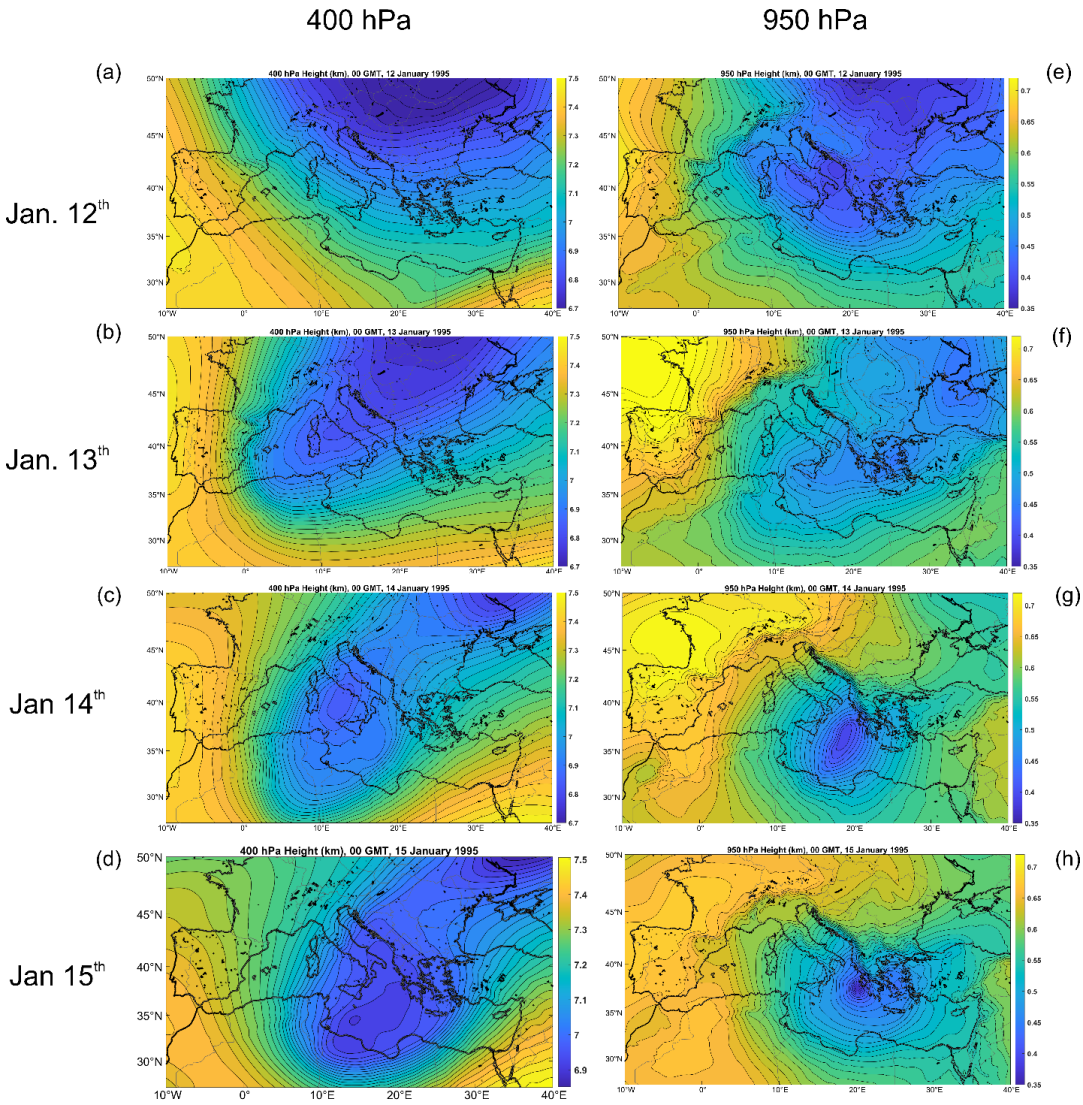
215 *Figure 3: Track of the surface center of the cyclone between 03:00 UTC on January 15 and 06:00 on January 18,*
 216 *1995, derived from satellite images (Pytharoulis et al., 1999)*

217 Figure 3 shows the track of the surface center of the cyclone, which developed between Greece
 218 and Sicily and made landfall in Libya. A detailed description of this medicane is provided by
 219 Pytharoulis et al. (1999).

220 The evolution of the system in increments of 24 hours, beginning on 00 GMT, 12 January and
 221 ending at 00 GMT 15 January, is shown in Figure 4. This sequence, showing the 400 hPa and
 222 950 hPa geopotential heights, covers the period just before the system develops. The evolution
 223 of the upper tropospheric (400 hPa) height field shows a classic Rossby wave breaking event
 224 (McIntyre and Palmer, 1983) in which an eastward-moving baroclinic Rossby wave at higher
 225 latitudes amplifies and irreversibly breaks to the south and west, finally forming a cut-off
 226 cyclone. To the southeast of this trough, a weak, broad area of low pressure develops at 950
 227 hPa mostly over land in a region of low-level warm advection. As the cold pool is gradually
 228 heated by the underlying sea, a broad surface cyclone develops by 00 GMT on January 14th. At
 229 around this time, the feedback between surface wind and surface enthalpy fluxes is strong
 230 enough to develop a tight inner warm core (warm, that is, relative to the surrounding cold pool,
 231 not necessarily to the unperturbed larger scale environment) by 00 GMT on January 15th,
 232 noticeable just to the west of northwestern Greece (Figure 5d). At the same time, the upper cold
 233 core weakens, no doubt aided by the strong heating from the surface transferred aloft by deep
 234 convection.



235



236

237 *Figure 4: Evolution of the 400 hPa (left) and 950 hPa (right) geopotential heights in 24-*
238 *hour increments, from 00 GMT 12 January to 00 GMT 15 January, 1995. These fields are*
239 *from ERA5 reanalysis. The 400 hPa heights span from 6.7 to 7.5 km, while the 950 hPa*
240 *heights range from 350 m to 730 m.*

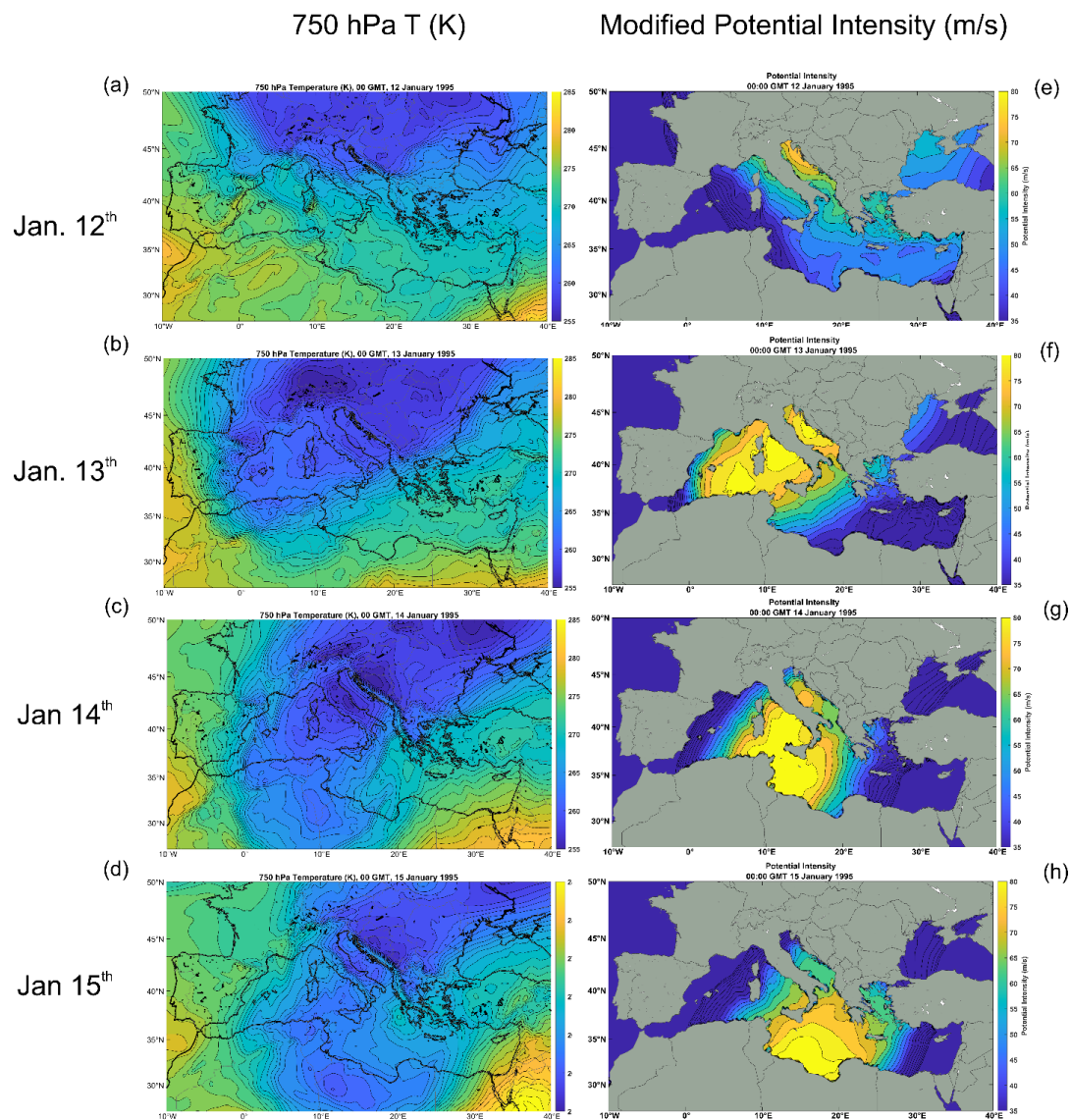


Figure 5: 750 hPa temperature (K; left) and modified potential intensity given by equation (1) (m/s, right) at 00 GMT on January 12th – 15th (top to bottom) 1995. The 750 hPa temperature spans from 255 K to 285 K, while the modified potential intensity ranges from 35 to 80 ms⁻¹. From ERA5 reanalysis.



Figure 5 shows the corresponding evolution of the 750 temperature and the modified potential intensity, V_{pm} , given by (1). The latter in this and subsequent figures is only shown in the range of 35 ms^{-1} to 80 ms^{-1} . Experience shows that tropical cyclone genesis is rare when the potential intensity is less than about 35 ms^{-1} (Emanuel, 2010).

On January 12th, relatively small values of V_{pm} are evident in the eastern and northern Mediterranean, but with higher values developing over the northern Adriatic as cold air aloft creeps in from the north. As the upper tropospheric Rossby wave breaks and a cut-off cyclone develops over the central Mediterranean, V_{pm} increase greatly during the 13th and 14th, with peak values greater than 80 ms^{-1} . The cyclop develops in a region of very high V_{pm} , though not where the highest values occur. Note that a lower warm core is not obvious at 750 hPa until January 15th and that it occurs on a somewhat smaller scale than the cut-off cyclone.

As the cyclop moves southward, it maintains a tight inner warm core until after landfall (not shown here) and the modified potential intensity, V_{pm} , over the south central Mediterranean diminishes rapidly, with peak values of only about 60 ms^{-1} by 00 GMT on January 17th. One potentially important difference between cyclop development and tropical transition is that in the former case, the volume of air with appreciable potential intensity is limited. It is possible that, by warming the whole tropospheric column relative to the surface, the enhanced surface fluxes associated with the cyclop substantially diminish the magnitude and/or volume of the high V_{pm} air, serving to limit the lifetime of the cyclop. This was the case in the axisymmetric numerical simulations of Emanuel (2005).

It is clear in this case that the cyclop development occurred on time and space scales appreciably smaller than those of the rather weak, synoptic-scale cyclogenesis resulting from the interaction of the positive PV perturbation near the tropopause with a low-level temperature gradient. It is also clear that the strong cooling of the troposphere in response to the development and southward migration of the cutoff cyclone aloft was instrumental in bringing about the high potential intensity necessary to activate the WISHE process. Therefore, the Rossby wave breaking did much more than trigger cyclogenesis; it provided the necessary potential intensity for the cyclop development. Here we draw a distinction from tropical transition, in which, in most cases, the pre-existing potential intensity suffices to maintain a surface flux-driven cyclone.

3.2 Medicane of December 2005

A medicane, unofficially known as Zeo, formed on December 14th 2005 off the coast of Tunisia and then moved eastward across a large stretch of the Mediterranean. Figure 6 shows a satellite image of this medicane on December 15th. This cyclone has been the subject of several intensive studies (e.g. Fita and Flaounas, 2018; Miglietta and Rotunno, 2019).

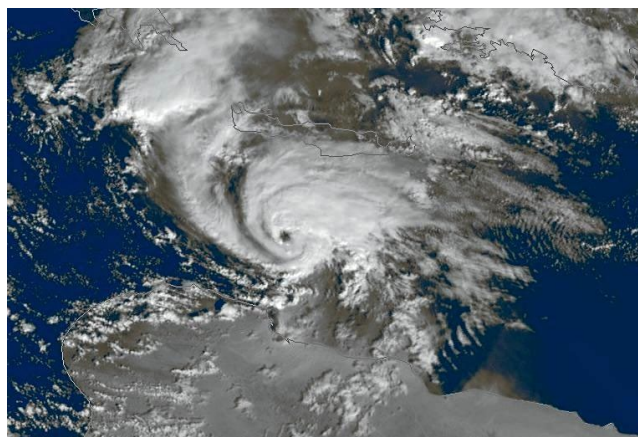
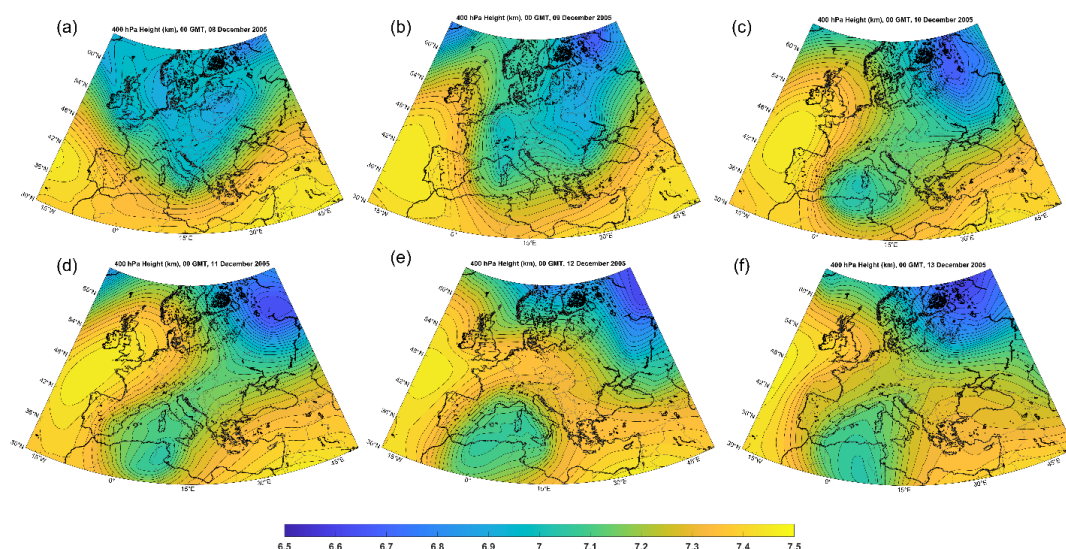


Figure 6: Mediane Zeo between Crete and Libya on 15 December 2005. Image from NASA.

Like Mediane Celeno, Mediane Zeo formed as a result of a Rossby wave breaking event, as illustrated in Figure 7. On December 8th (panel a), a deep trough is digging southward over eastern Europe, but by the 9th (panel b) it has split in two, with the westward half breaking southwestward over Germany and Switzerland. By the 11th (panel d), this local minimum is located over Tunisia and on the 12th (panel e) is more or less completely cut off from the main westerly jet. It subsequently oscillates over Tunisia and Algeria, before moving slowly eastward over the Mediterranean, as shown in Figure 8.

In response to the cutoff cyclone development, a broad, synoptic-scale surface cyclone formed to the east of the upper cyclone over the deserts of Libya during December 12th and 13th (not shown here). The poorly defined center of this system drifted northward, on collision course with the upper cyclone, which was drifting eastward over Tunisia by late on the 13th. As the surface center moved out over the Mediterranean early on the 13th, rapid development ensued and a mature cyclop was evident by 00 GMT on the 14th (Figure 8c). The system began to move eastward and reached peak intensity on the 14th (lower panels of Figure 8). The cyclop moved eastward, along with its parent upper cyclone, and dissipated in the far eastern Mediterranean on the 16th (not shown).

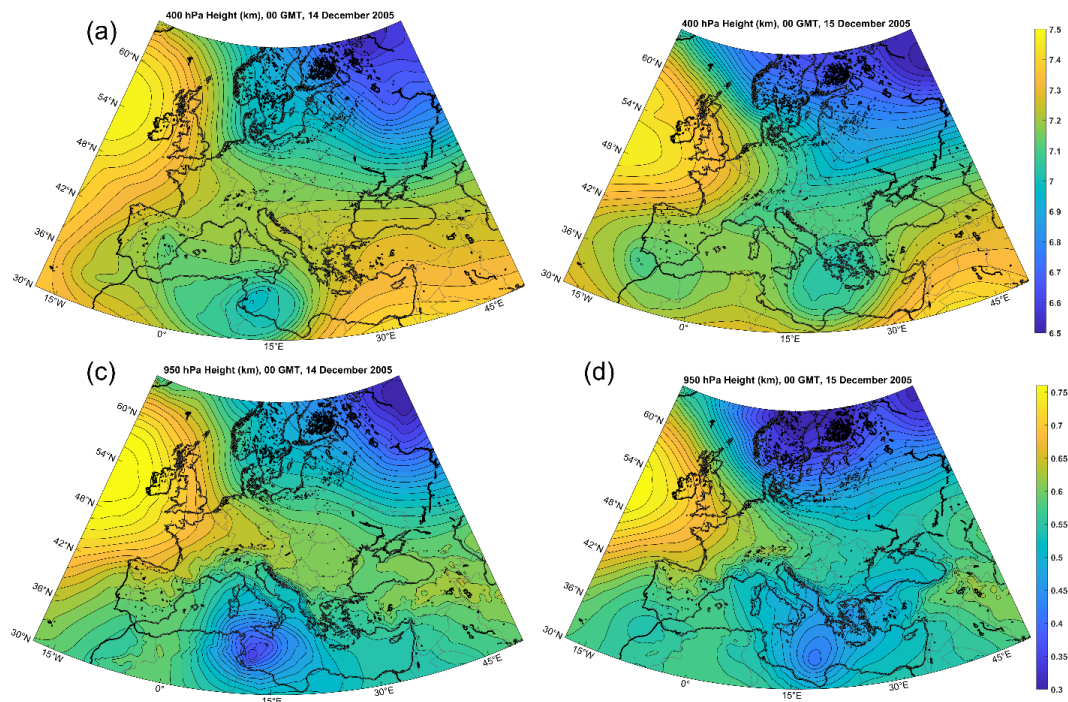


302

303 *Figure 7: 400 hPa geopotential heights, ranging from 6.5 km to 7.5 km (color scale identical for all panels) at 00 GMT*
 304 *on December 8th (a), 9th (b), 10th (c), 11th (d), 12th (e), and 13th (f), 2005. From ERA-5 reanalysis.*

305 The evolutions of 750 hPa temperature and V_{pm} on the 14th and 15th of December are shown in
 306 Figure 9. In this case, there were large meridional gradients of sea surface temperature across
 307 the Mediterranean, ranging from over 20°C in the far south to less than 12°C in the northern
 308 reaches of the Adriatic and western Mediterranean (not shown here). As the cold pool moved
 309 southwestward and deepened, only low values of V_{pm} are present over the northern
 310 Mediterranean, but beginning on December 10th, higher values developed over the Gulf of
 311 Sidra, east of Tunisia, and by the 14th (Figure 9c) had reached at least 80 ms⁻¹, enabling the
 312 formation of the cyclop. As in the Celeno case, V_{pm} values diminish thereafter, possibly
 313 because of the surface enthalpy flux.

314

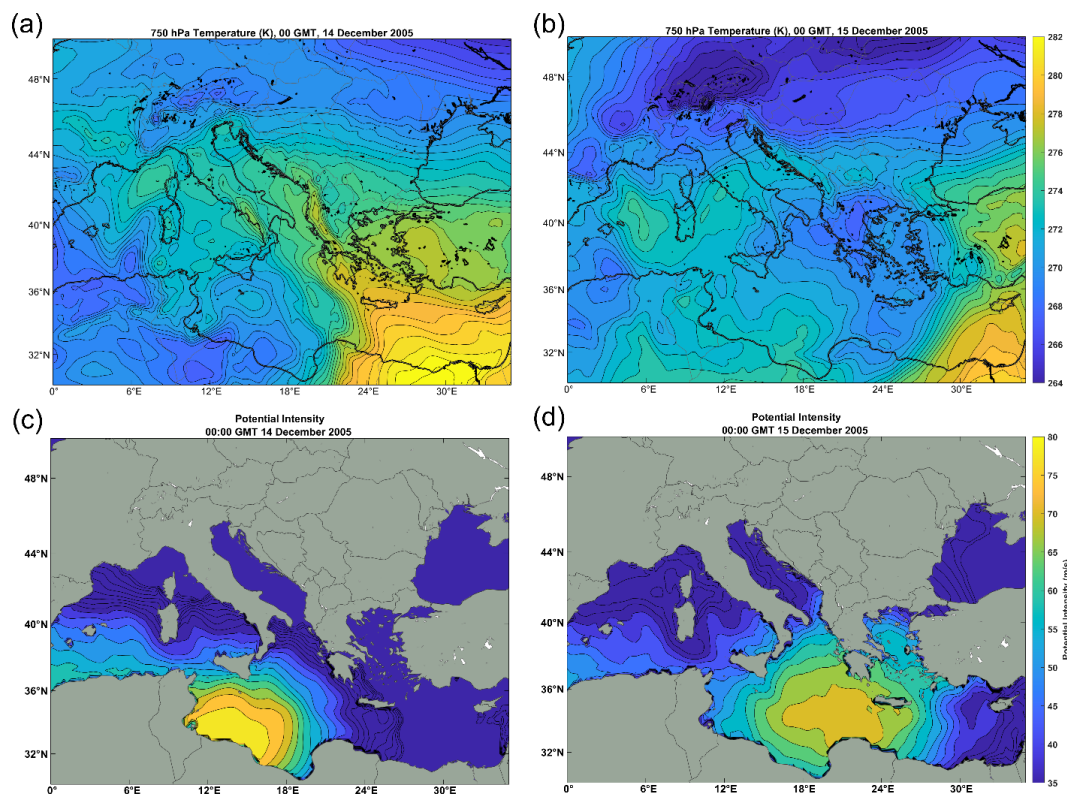


315
316 *Figure 8: Evolution of 400 hPa geopotential height, ranging from 6.5 to 7.5 km (a and b), and 950 hPa geopotential*
317 *height, ranging from 250 to 750 m (c and d) at 00 GMT in December 14th (left) and 15th (right), 2005. The color scales*
318 *of (a) and (b) are identical, as are the color scales of (c) and (d). From ERA-5 reanalysis.*

319
320



321



322

323 *Figure 9: 750 hPa temperature (K; a-b) and modified potential intensity ($m s^{-1}$, c-d) at 00 GMT on December 14th (a,c)*
 324 *and December 15th (b,d) 2005. From ERA-5 reanalysis.*

325 The 750 hPa temperature field (Figure 9a) shows a complex pattern of positive temperature
 326 perturbation near the position of the surface low, not nearly as focused as in the case of
 327 medicane Celeno. As suggested by Fita and Flaounas (2018), part of the positive temperature
 328 anomaly associated with the cyclone may have resulted from a warm seclusion. Yet 24 hours
 329 later (Figure 9b) the warm anomaly near the cyclone center over the eastern Gulf of Sidra
 330 appears to have been advected from the south rather than the north. It is possible that the
 331 reanalysis did not capture the full physics of this particular medicane.

332 Figure 10 compares total column water retrieved from satellite microwave and near-infrared
 333 imagers (a) to that from the ERA5 reanalysis (b). While there is some broad agreement between
 334 the two estimates, the ERA5 underestimates column water in the critical region just east of
 335 Tunisia and overestimates it in an arc extending from eastern Sicily southeastward to the Libyan
 336 coast. Cyclop intensity, in analogy to tropical cyclone intensity, should be highly sensitive to
 337 moisture in the mesoscale inner core region, and may be under-resolved and otherwise not well
 338 simulated by global NWP models. For this reason, we do not routinely show reanalysis of water
 339 vapor in this paper.

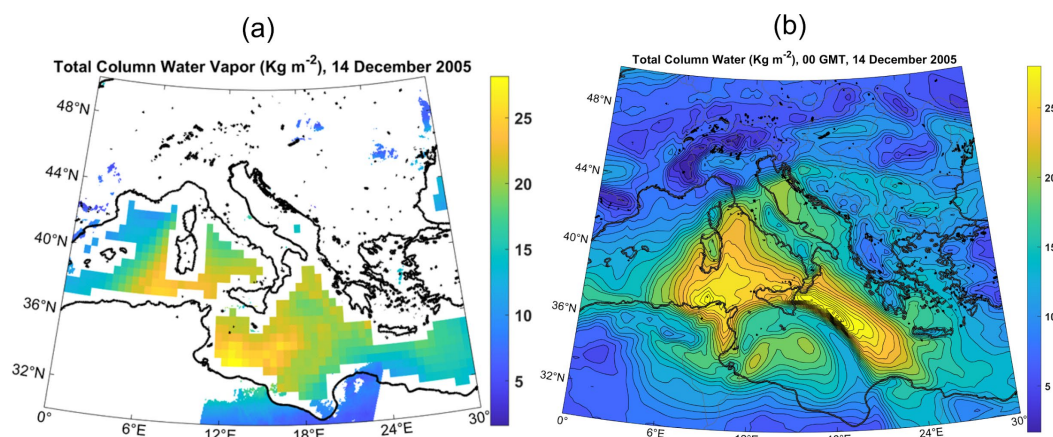
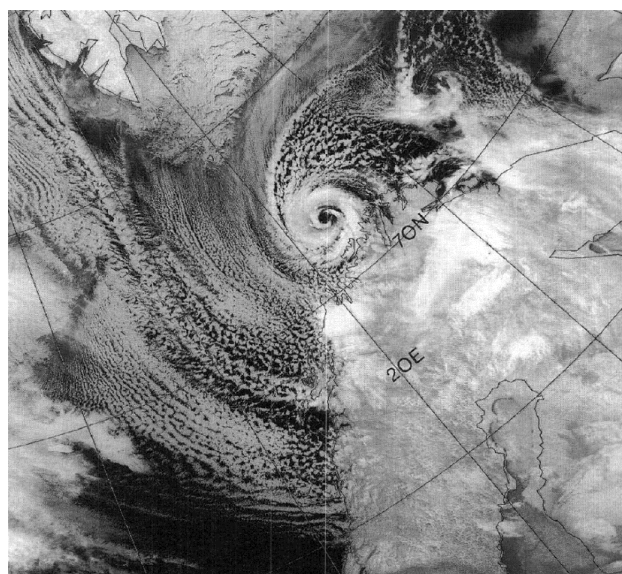


Figure 10: Total column water vapor (Kg m^{-2}) at 00 GMT on 14 December 2005, derived from microwave and near infrared imagers (a) and ERA5 reanalysis (b).

3.3 Polar low of February, 1987

Closed upper tropospheric lows also provide favorable environments for cyclop development at very high latitudes in locations where there is open water. These usually form poleward of the mid-latitude jet, where quasi-balanced dynamics can be quite different from those operating at lower latitudes. Figure 11 is an infrared image of a polar low that formed just south of Svalbard on February 25th, 1987, and tracked southward, making landfall on the north coast of Norway on the 27th. This system was studied extensively by Nordeng and Rasmussen(1992).



351

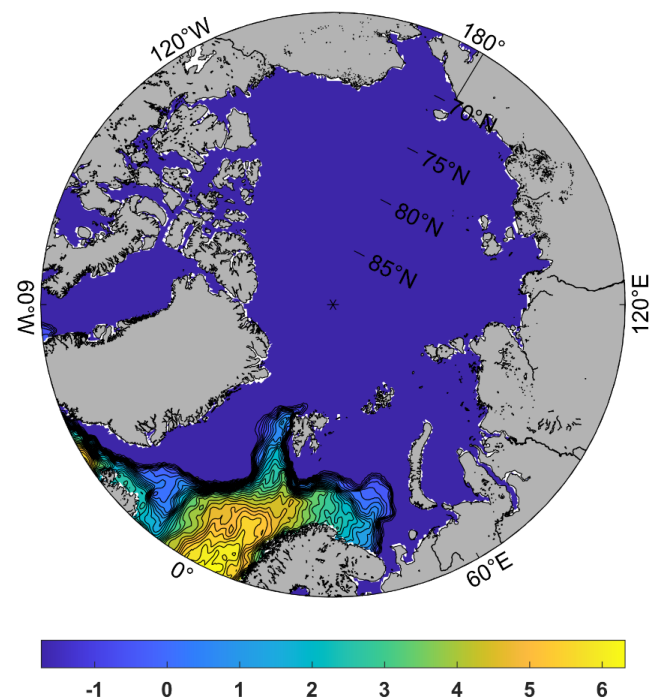
352 *Figure 11: NOAA 9 satellite infrared image (channel 4) of a polar low just north of Norway at 08:31 GMT on 27*
 353 *February 1987.*

354 As with medicanes, polar lows develop in strongly convecting air masses when cold air moves
 355 out over relatively warm water. The adjective “relatively” is crucial here; with polar lows the sea
 356 surface temperature is often only marginally above the freezing point of saltwater. Figure 12
 357 shows the distribution of sea surface temperature on February 25th, with the uniform dark blue
 358 areas denoting regions of sea ice cover. The polar low shown in Figure 11 develops when deep
 359 cold air moves southward over open water, as shown in Figure 13.

360 In this case, it is not clear whether one can describe what happens in the upper troposphere
 361 (top row of Figure 13) as a Rossby wave breaking event. Instead, what we see is a complex
 362 rearrangement of the tropospheric winter polar vortex, as a ridge building over North America
 363 breaks and forms an anticyclone over the North Pole. This complex rearrangement results in the
 364 formation of a deep cutoff low just south of Svalbard by the 26th, which then moves southward
 365 over Norway by the 27th. The polar low is barely visible in the 950 hPa height field on the 25th
 366 (middle row of Figure 13), but intensifies rapidly as it moves over progressively warmer water,
 367 reaching maturity before landfall on the 27th.



368

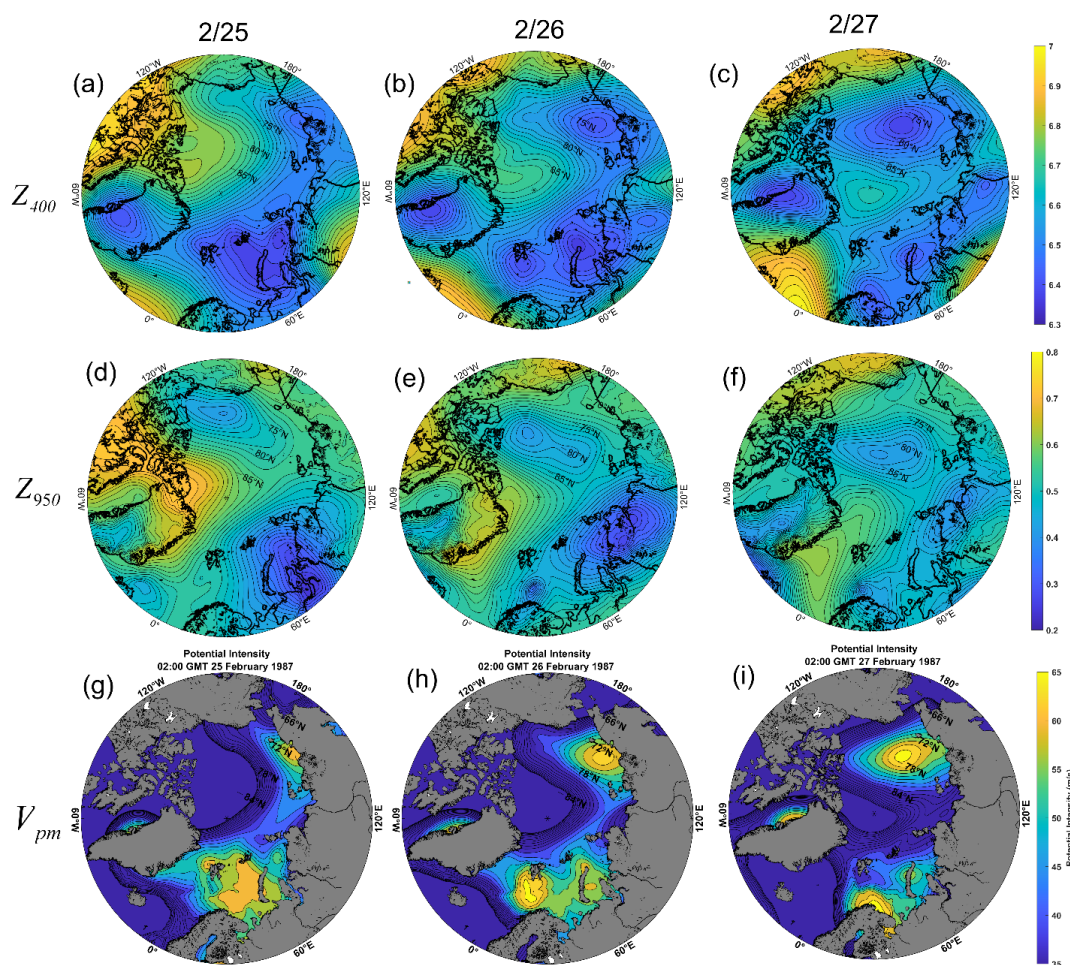


369

370 *Figure 12: Sea surface temperature (°C) at 02:00 GMT on 25 February, 1987, from ERA5 reanalysis. Dark blue*
371 *areas denote regions of sea ice. From ERA-5 reanalyses.*

372 The evolution of the V_{pm} field is shown in the bottom row of Figure 13. The potential intensity
373 increases rapidly south of Svalbard as the cut-off cyclone moves out over open water.

374 Under these conditions, almost all the surface flux that drives the cyclop is in the form of
375 sensible, rather than latent heat flux, and the background state has a nearly dry (rather than
376 moist) adiabatic lapse rate. As shown by Cronin and Chavas (2019) and Velez-Pardo and
377 Cronin (2023), surface flux-driven cyclones can develop in perfectly dry convecting
378 environments, though they generally reach smaller fractions of their potential intensity and lack
379 the long tail of the radial profile of azimuthal winds that is a consequence of the dry stratification
380 resulting from background moist convection (Chavas and Emanuel, 2014). They also have
381 larger eyes relative to their overall diameters. Given the low temperatures at which they occur,
382 polar lows may be as close to the Cronin-Chavas dry limit as one might expect to see in Earth's
383 climate.



384

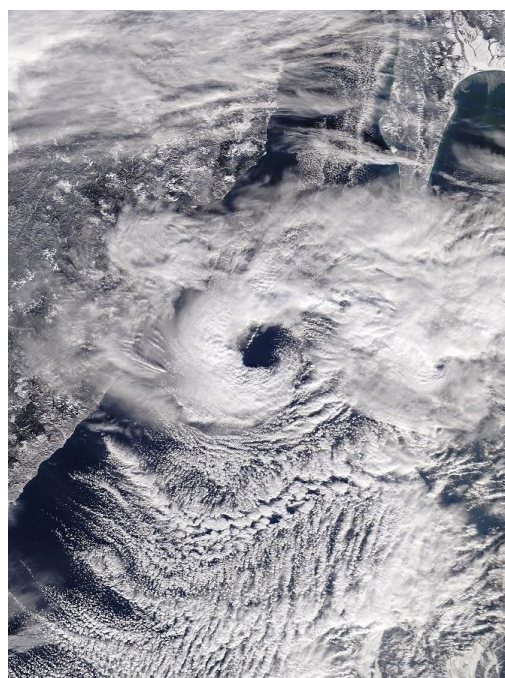
385 *Figure 13: 400 hPa geopotential height (km; a-c), 950 hPa geopotential height (km; d-f), and V_{pm} (ms^{-1} ; g-i), at 02:00*
 386 *GMT on February 25th (left), 26th (center), and 27th (right), 1987. From ERA-5 reanalysis.*

387 One interesting feature of polar waters in winter is that the thermal stratification is sometimes
 388 reversed from normal, with warmer waters lying beneath cold surface waters. This is made
 389 possible, in part, by strong salinity stratification, that keeps the cold water from mixing with the
 390 warmer waters below. Therefore, it is possible for polar lows to generate warm, rather than cold,
 391 wakes, and this would feed back positively on their intensity. This seems to happen in roughly
 392 half the documented cases of polar lows in the Nordic seas (Tomita and Tanaka, 2024).



393 3.4 Polar low over the Sea of Japan, December, 2009

394 Polar lows are not uncommon in the Sea of Japan, forming when deep, cold air masses from
 395 Eurasia flow out over the relatively warm ocean. They are frequent enough to warrant a
 396 climatology (Yanase and co-authors, 2016). A satellite image of one such storm is shown in
 397 Figure 14.



398

399 *Figure 14: Polar low over the northern Sea of Japan, 02:13 GMT 20 December, 2009 as captured by the MODIS*
 400 *imager on NASA's Terra satellite.*

401 The cyclone traveled almost due south from this point, striking the Hokkaido region of Japan,
 402 near Sapporo, with gale-force winds and heavy snow. As with other cyclops, it formed in an
 403 environment of deep convection under a cold low aloft.

404 The development of the cutoff cyclone aloft was complex, as shown by the sequence of 400
 405 hPa maps displayed in Figure 15. These are 00 GMT charts at 1-day intervals beginning on
 406 December 11th and ending on the 20th, about the time of the image in Figure 14. A large polar
 407 vortex is centered in northern central Russia on the 11th but sheds a child low southeastward on
 408 the 12th and 13th, becoming almost completely cutoff on the 14th. The parent low drifts westward
 409 during this time. The newly formed cutoff cyclone meanders around in isolation from the 15th
 410 through the 17th, but becomes wrapped up with a system propagating into the domain from the
 411 east on the 18th. By the 20th, a small-scale cutoff cyclone is drifting southward over the northern
 412 Sea of Japan, and it is this upper cutoff that spawns the polar low.

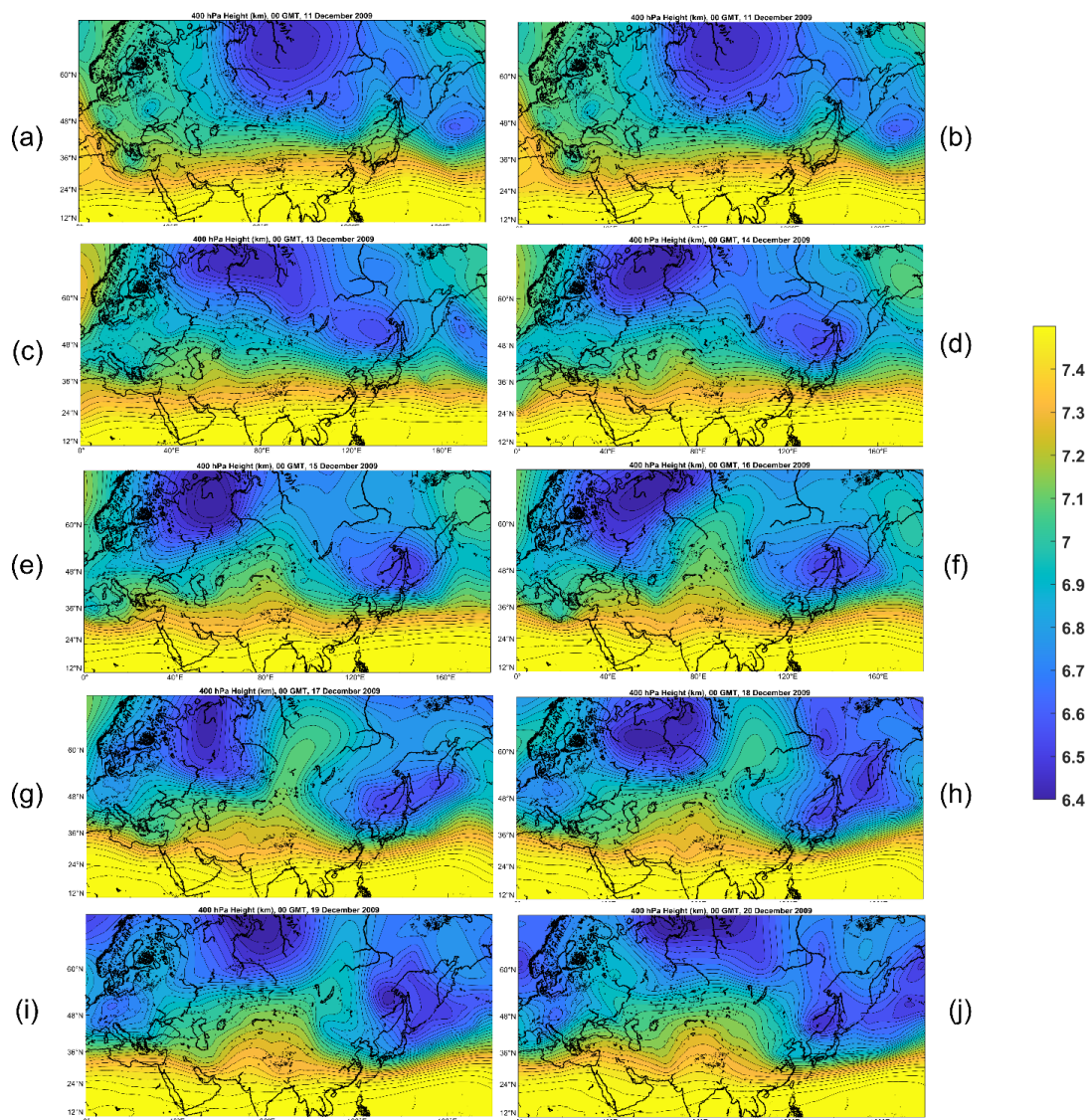
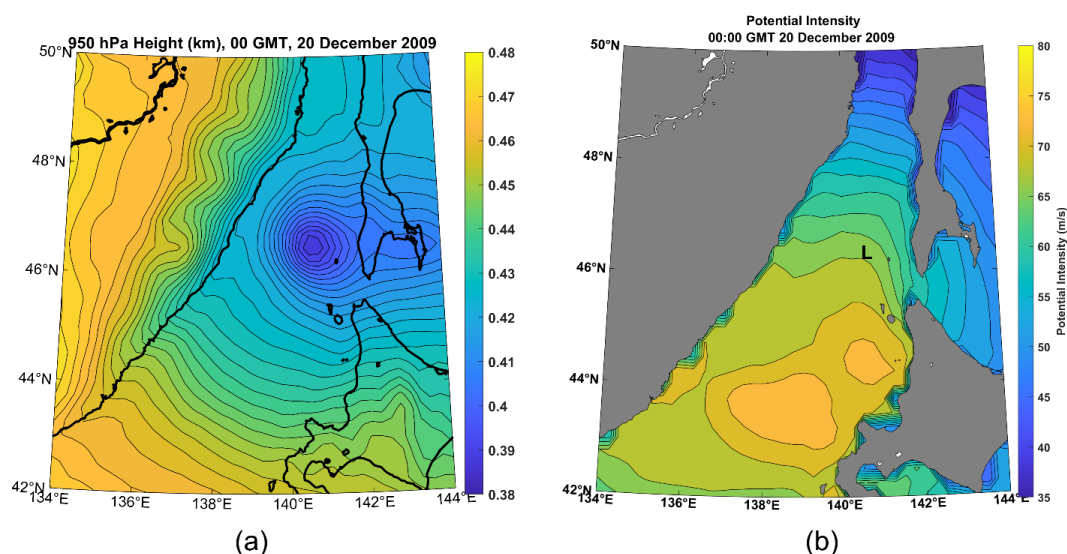


Figure 15: Sequence of 400 hPa geopotential height (km) charts at 1-day intervals from 00 GMT on December 11th (a) to 00 GMT on December 20th (j), 2009. The charts span from 0° to 180° longitude and from 10° to 70° latitude. From ERA-5 reanalysis.



419 The 950 hPa height and the V_{pm} fields at 00 GMT on December 20th are shown in Figure 16. At
 420 this time, the surface low is developing rapidly and moving southward into a region of high
 421 potential intensity. The latter reaches a maximum near the northwest coast of Japan, where the
 422 sea surface temperatures are larger. As with the two medicane cases and the other polar low
 423 case, the cyclop develops in a place where the potential intensity values are normally too low for
 424 surface flux-driven cyclones but for which the required potential intensity is created by the
 425 approach of a deep cold cyclone aloft. The reanalysis 750 hPa temperature (not shown)
 426 presents a local maximum at the location of the surface cyclone at this time.



427 (a) (b)
 428 Figure 16: 950 hPa geopotential height (a; km) and V_{pm} (b) at 00 GMT on 20 December, 2009. In (b), the “L” marks
 429 the satellite-derived surface cyclone center. From ERA-5 reanalysis.

431 3.5 The subtropical cyclone of January, 2023

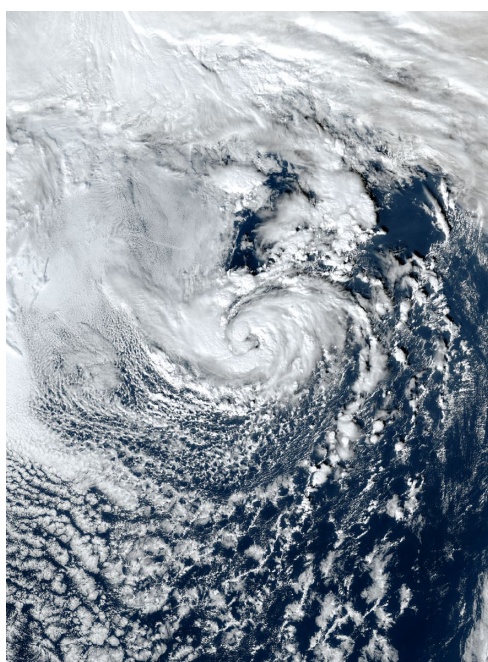
432 The term “subtropical cyclone” has been used to describe a variety of surface flux-assisted
 433 cyclonic storms that do not strictly meet the definition of a tropical cyclone. The term has an
 434 official definition in the North Atlantic⁴ but is used occasionally elsewhere, especially in regions
 435 where terms like medicane, polar low, and Kona storm do not apply, such as the South Atlantic
 436 (Evans and Braun, 2012; Gozzo et al., 2014). Here we will use the term to designate cyclops in
 437 the sub-arctic North Atlantic; that is, surface flux-powered cyclones that develop in regions and
 438 times whose climatological thermodynamic potential is small or zero, that would not be called

⁴ The National Hurricane Center defines a “subtropical cyclone” as “a non-frontal low-pressure system that has characteristics of both tropical and extratropical cyclones”, but in the past has also used the terms “hybrid storm” and “neutercane”.



439 polar lows owing to their latitude. This usage may not be consistent with other definitions. The
 440 point here is to show that cyclops can occur in the North Atlantic and we can safely refer to
 441 these as cyclops whether or not they meet some definition of “subtropical cyclone”.

442 Figure 17 displays a visible satellite image of a subtropical cyclone over the western North
 443 Atlantic on 16 January, 2023. It resembles the medicanes and polar lows described previously,
 444 and like them, formed under a cutoff cyclone aloft.



445

446 *Figure 17: Subtropical cyclone over the western North Atlantic, 18:20 GMT, 16 January 2023. NOAA geostationary*
 447 *satellite image.*

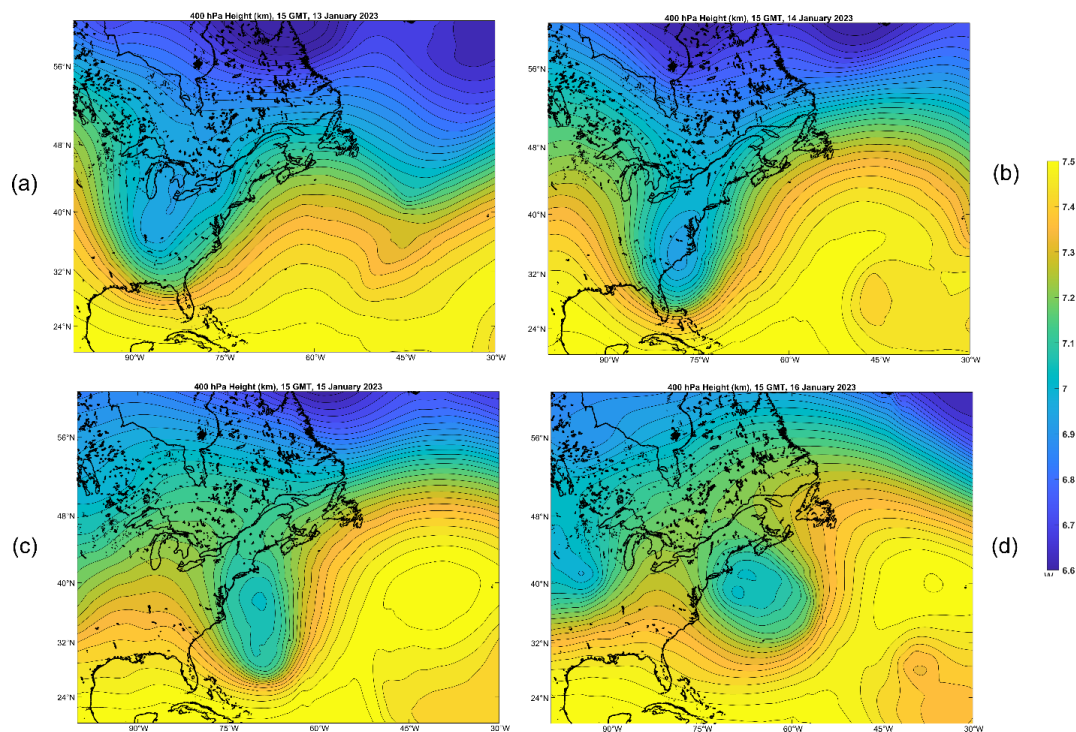
448 The formation of the cutoff cyclone aloft is shown in Figure 18. A deep trough advances slowly
 449 eastward over eastern North America and partially cuts off on the 14th. As the associated cold
 450 pool and region of light shear migrate out over the warm waters south of the Gulf Stream, a
 451 cyclop forms and intensifies with peak winds of around 60 kts at around 00 GMT on the 17th
 452 (Canglioni et al., 2023). Note also the anticyclonic wave breaking event to the east of the
 453 surface cyclone development.

454 The evolutions of the 950 hPa and associated V_{pm} fields are displayed in Figure 19. (Note the
 455 smaller scale around the developing surface cyclone, compared to Figure 18.) On January 14th,
 456 the only appreciably large values of V_{pm} are in the Gulf Stream and in the far southwestern
 457 portion of the domain. The 950 hPa height field shows a broad trough associated with the
 458 baroclinic wave moving slowly eastward off the U.S. east coast. But as the upper cold cyclone



459 moves out over warmer water on the 15th, large V_{pm} develops south of the Gulf Stream, and a
 460 closed and more intense surface cyclone develops under the lowest 400 hPa heights and over
 461 the region with higher V_{pm} values.

462



463

464 *Figure 18: 400 hPa geopotential height (km) at 15:00 GMT on January 13th (a), 14th (b), 15th (c), and 16th (d), 2023.*
 465 *From ERA-5 reanalysis.*

Figure 1 consists of six panels (a-f) showing potential intensity and 950 hPa height over the North Atlantic. Panels (a-c) show potential intensity at 00, 15, and 18 GMT on Jan 14, 2023. Panels (d-f) show 950 hPa height at the same times. A color bar on the right indicates potential intensity from 0.35 to 0.7.

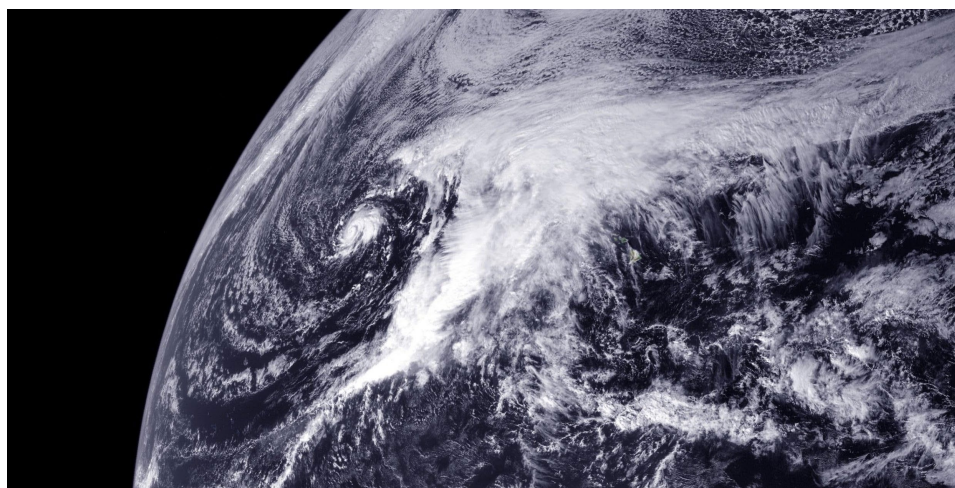
As the upper tropospheric cyclone begins to pull out toward the northeast on the 16th, the surface cyclone intensifies in the region of large V_{pm} south of the Gulf Stream, while the more gradual warming of the surface air in the region of small V_{pm} north of the Stream yields surface pressure falls, but not as concentrated and intense as in the cyclop to the south.

Although the evolution of the upper tropospheric cyclone differs in detail from the previously examined cases, and the sharp gradient of sea surface temperature across the north wall of the Gulfstream clearly plays a role here, in other respects the development of this subtropical cyclone resembles that of other cyclops, developing in regions of substantial thermodynamic potential that result from cooling aloft on synoptic time and space scales.

Hawaiians use the term “Kona Storm” to describe cold-season storms that typically form west of Hawaii and often bring damaging winds and heavy rain to the islands. The term “Kona” translates to “leeward”, which in this region means the west side of the islands. They may have been first described in the scientific literature by Daingerfield (1921). Simpson (1952) states that Kona Storms possess “cold-core characteristics, with winds and rainfall amounts increasing with distance from the low-pressure center and reaching a maxima at a radius of 200 to 500 mi. However, with intensification, this cyclone may develop warm-core properties, with rainfall and wind profiles bearing a marked resemblance to those of the tropical cyclone.” In general,



489 Simpson's descriptions of the later stages of some Kona Storms are consistent with them being
490 cyclops. But it should be noted that the term is routinely applied to cold-season storms that
491 bring hazardous conditions to Hawaii regardless of whether they have developed warm cores.
492 Here we focus on those that do, providing as a single example the Kona Storm of 19 December
493 2010. A visible satellite image of this storm is shown in Figure 20.



494

495 *Figure 20: Geostationary satellite visible image showing a Kona Storm at 00 GMT on 19 December 2010. The Kona*
496 *Storm is the small-scale cyclone left of the major cloud mass. (Image credit: NOAA-NASA GOES Project, 2010.)*

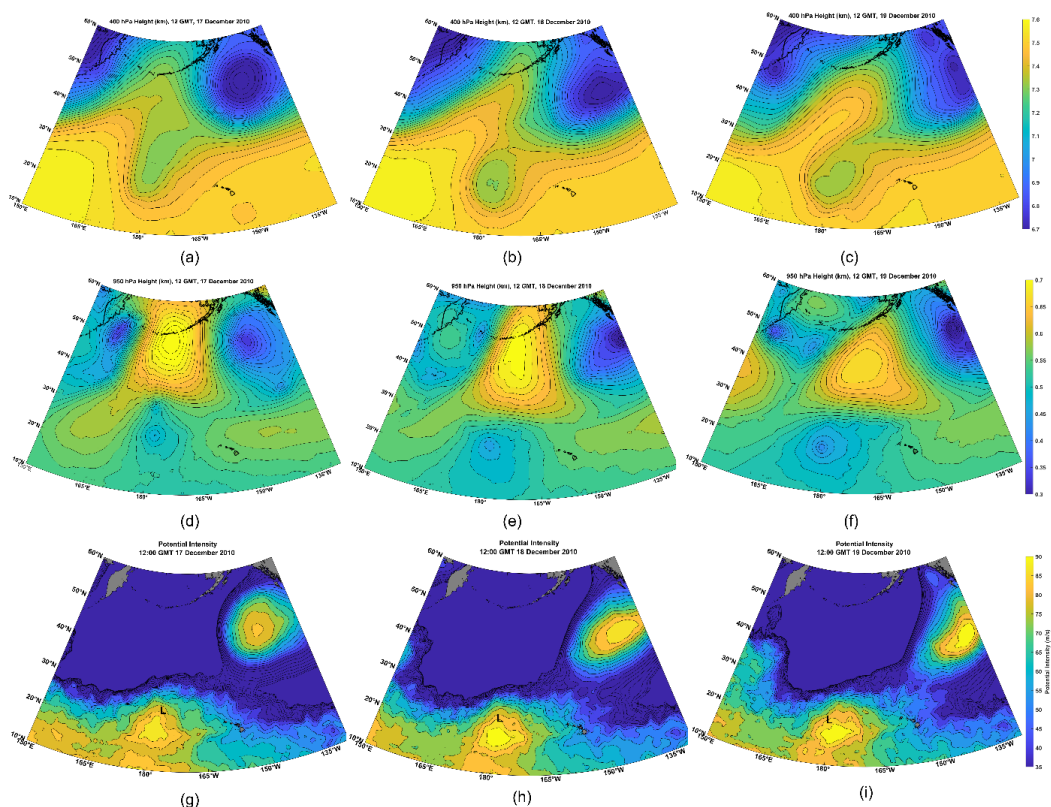


Figure 21: Sequence of 400 hPa geopotential height charts (km; (a)-(c)), 950 hPa geopotential heights (km; (d)-(f)), and V_{pm} ((g)-(i)) at 12:00 GMT on December 17th ((a), (d), (g)), December 18th ((b), (e), (h)), and December 19th ((c), (f), (i)) 2010. The “L”s in ((g)-(i)) denote the positions of the 950 hPa cyclone center. From ERA-5 reanalysis.

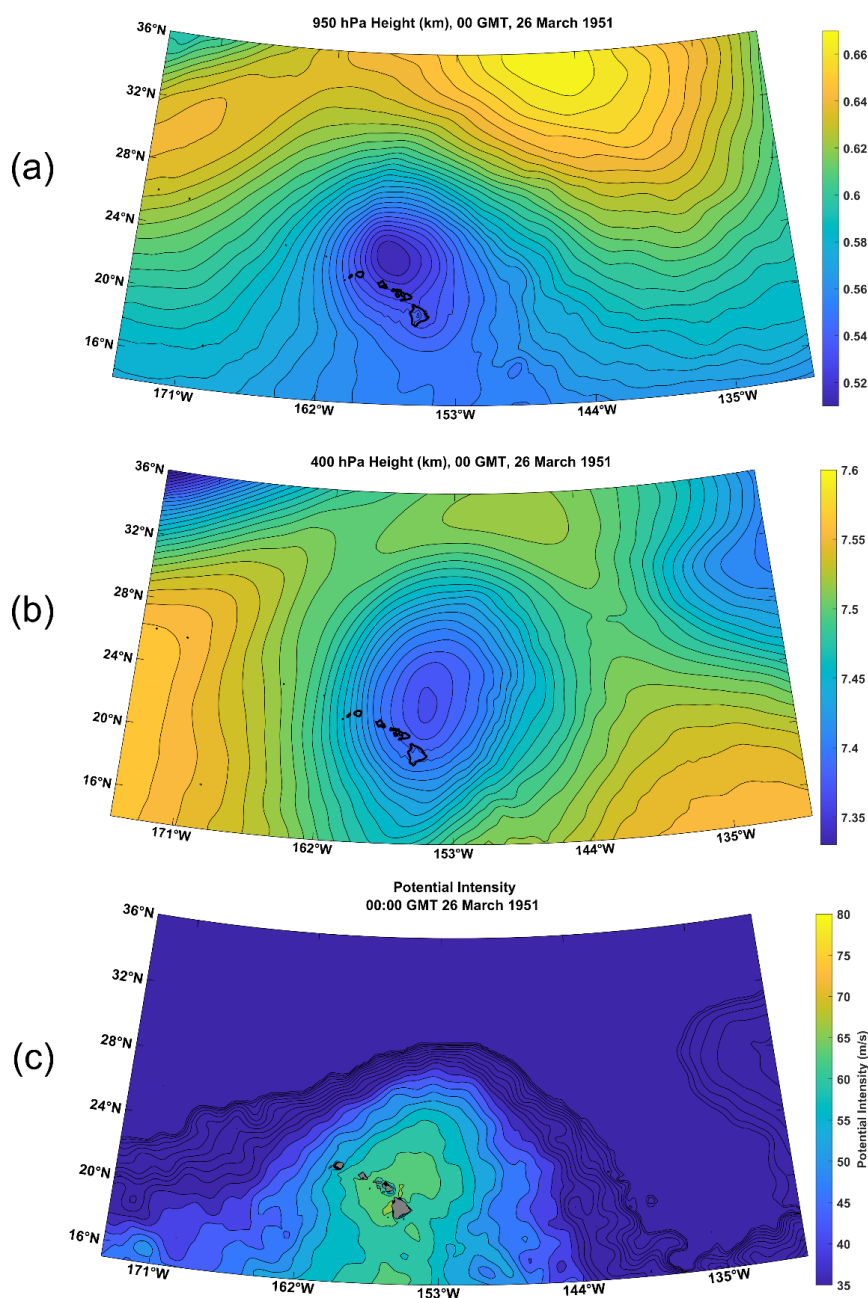
As with all known cyclops, the December 2010 Kona Storm developed under a cold-core cutoff cyclone aloft, as shown in Figure 21. The upper-level cyclone had a long and illustrious history before December 18th, having meandered over a large swath of the central North Pacific. But beginning on December 17th, the cutoff cyclone made a decisive swing southward over waters with higher values of V_{pm} . A broad surface cyclone was present underneath the cold pool aloft on all three days, but developed a tight inner core on the 19th as the cold pool slowly drifted over a region of higher potential intensity.

This Kona Storm developed in a region of modest climatological potential intensity that was, however, substantially enhanced by the cutoff cyclone aloft. For example, on December 17th, the conventional (unmodified) potential intensity at the position of the 950 hPa cyclone center was about 55 ms⁻¹, compared to the 75-80 ms⁻¹ values of the modified potential intensity. One can only speculate whether a surface flux-driven cyclone would have developed without the enhanced cooling associated with the cutoff cyclone aloft.



514

515 Figure 22 shows the 950 hPa geopotential height field of another Kona Storm, that of March,
516 1951. The storm, at that time, was classified by the Joint Typhoon Warning Center as a tropical
517 cyclone, but the climatological potential intensity there at that time of year could not have
518 supported any tropical cyclone. Figure 22c shows that substantial V_{pm} was associated with a
519 cutoff cyclone in the upper troposphere, making possible the existence of a cyclop.



520

521 *Figure 22: Kona Cyclone of March, 1951. Fields are shown at 00 GMT on 26 March: a): 950 hPa geopotential height*
 522 *(km), b): 400 hPa geopotential height (km), and c): V_{pm} .*



523 4. Variations on the Theme

524 We here are attempting to distinguish a class of cyclones, cyclops, from other cyclonic storms
 525 by their physics, not by the regions in which they develop. Here we present a case of an actual
 526 tropical cyclone in the Mediterranean that we do not identify as a cyclop.

527 4.1 Cyclone Zorbas

528 The cyclone known as Zorbas developed just north of Libya on 27 September 2018 and moved
 529 northward and then northeastward across the Peloponnese and the Aegean (Figure 23).
 530 dissipating in early October. The storm killed several people and did millions of dollars of
 531 damage.



532

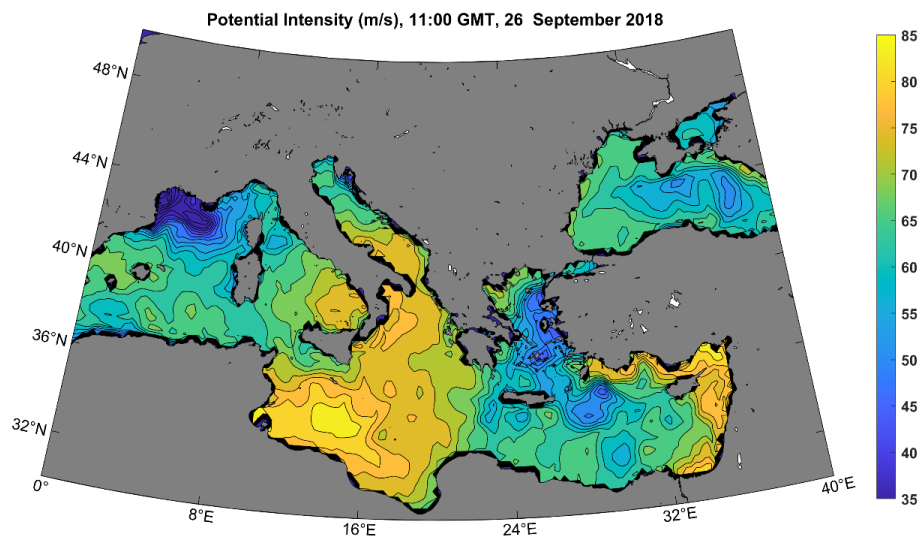
533 *Figure 23: Track of Cyclone Zorbas, from 27 September through 2 October, 2018. (Image credit: Wikipedia*
 534 *Commons; https://commons.wikimedia.org/wiki/File:Zorbas_2018_track.png)*

535 The antecedent (actual, not modified) potential intensity distribution, on 26 September, is
 536 displayed in Figure 24. In much of the Mediterranean, the potential intensity was typical of
 537 tropical warm pools with values approaching 80 ms^{-1} . As with most medicanes, Zorbas was
 538 triggered by an upper tropospheric Rossby wave breaking event (Figure 25), but in this case the
 539 cold pool aloft only enhanced the existing potential intensity by about 7 ms^{-1} (on September
 540 27th.) In this case, the maximum 400 hPa geopotential perturbation was around $1500 \text{ m}^2\text{s}^{-2}$,
 541 compared to about $2500 \text{ m}^2\text{s}^{-2}$ in the case of Medicanes Zeo of 2005. Zorbas was therefore more
 542 like a classic case of a tropical cyclone resulting from tropical transition (Bosart and Bartlo,
 543 1991; Davis and Bosart, 2003, 2004) and we would not describe it as a cyclop. Note that while
 544 the approach of the upper-level cyclone did not appreciably alter the potential intensity, it almost
 545 certainly humidified the middle troposphere, making genesis somewhat more likely.

546



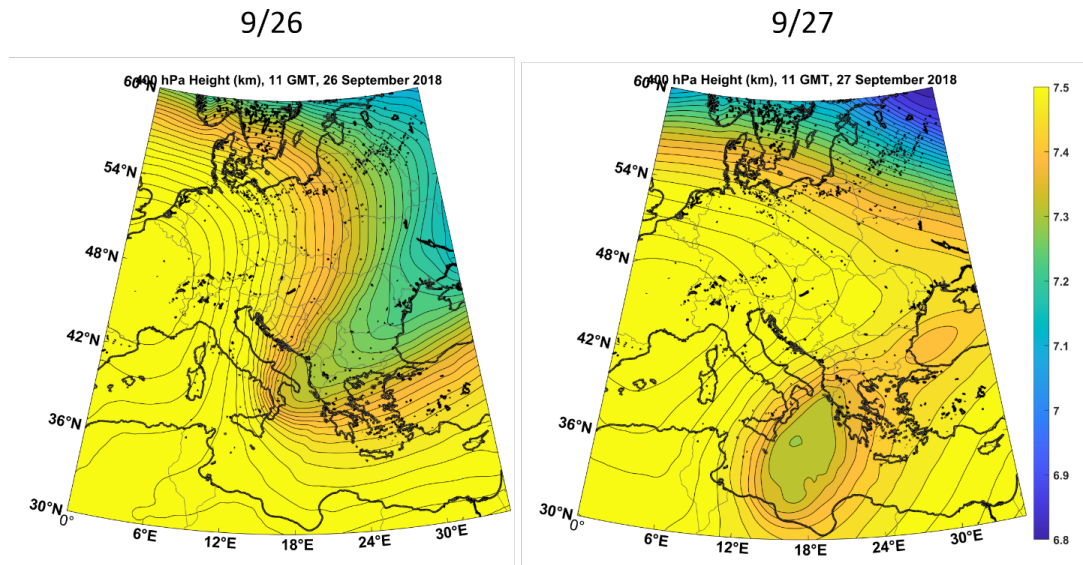
547



548

549 Figure 24: Potential intensity distribution in the Mediterranean and Black Seas, 11 GMT on 26 September 2018.

550



551

552 Figure 25: 400 hPa geopotential height (km) at 11 GMT on 26 September (left) and 27 September (right), 2018, from
553 ERA-5 reanalysis.



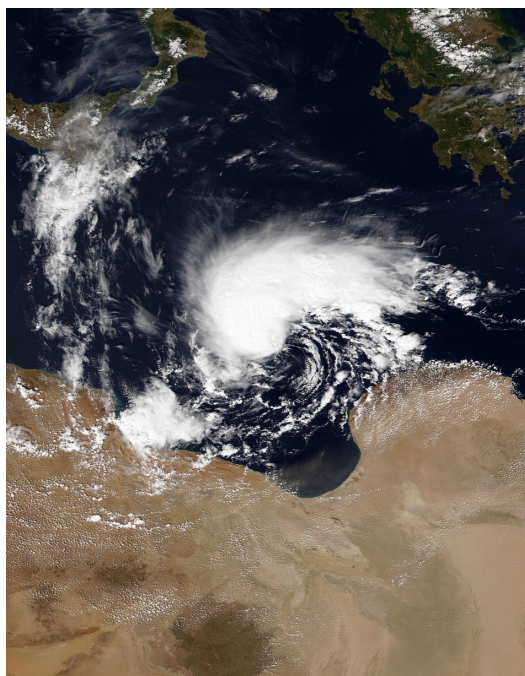
554 4.2 Cyclone Daniel

555 Cyclone Daniel of 2023 was the deadliest Mediterranean surface flux-driven cyclone in recorded
 556 history, with a death toll exceeding 4,000 and thousands of missing persons, mostly owing to
 557 floods caused by the catastrophic failure of two dams near Derna, Libya (Flaounas et al., 2024).
 558 This flooding was the worst in the recorded history of the African continent. Figure 26 shows the
 559 track of Daniel's center and a visible satellite image of the storm as it approached landfall in
 560 Libya is shown in Figure 27. Daniel became a surface flux-driven cyclone off the west coast of
 561 the Peloponnese on September 5th, made landfall near Benghazi, Libya, on September 10th and
 562 dissipated over Egypt on the 12th.



563

564 *Figure 26: Track of Storm Daniel at 6-hour intervals, beginning September 5th and ending September 12th, 2023. The*
 565 *circles, squares and triangles along the track denote tropical cyclone, subtropical cyclone and extratropical cyclone*
 566 *designations, respectively, while the deep blue and light blue colors denote tropical depression- and tropical storm-*
 567 *force winds. (Image credit: Wikipedia commons; https://commons.wikimedia.org/wiki/File:Daniel_2023_track.png)*

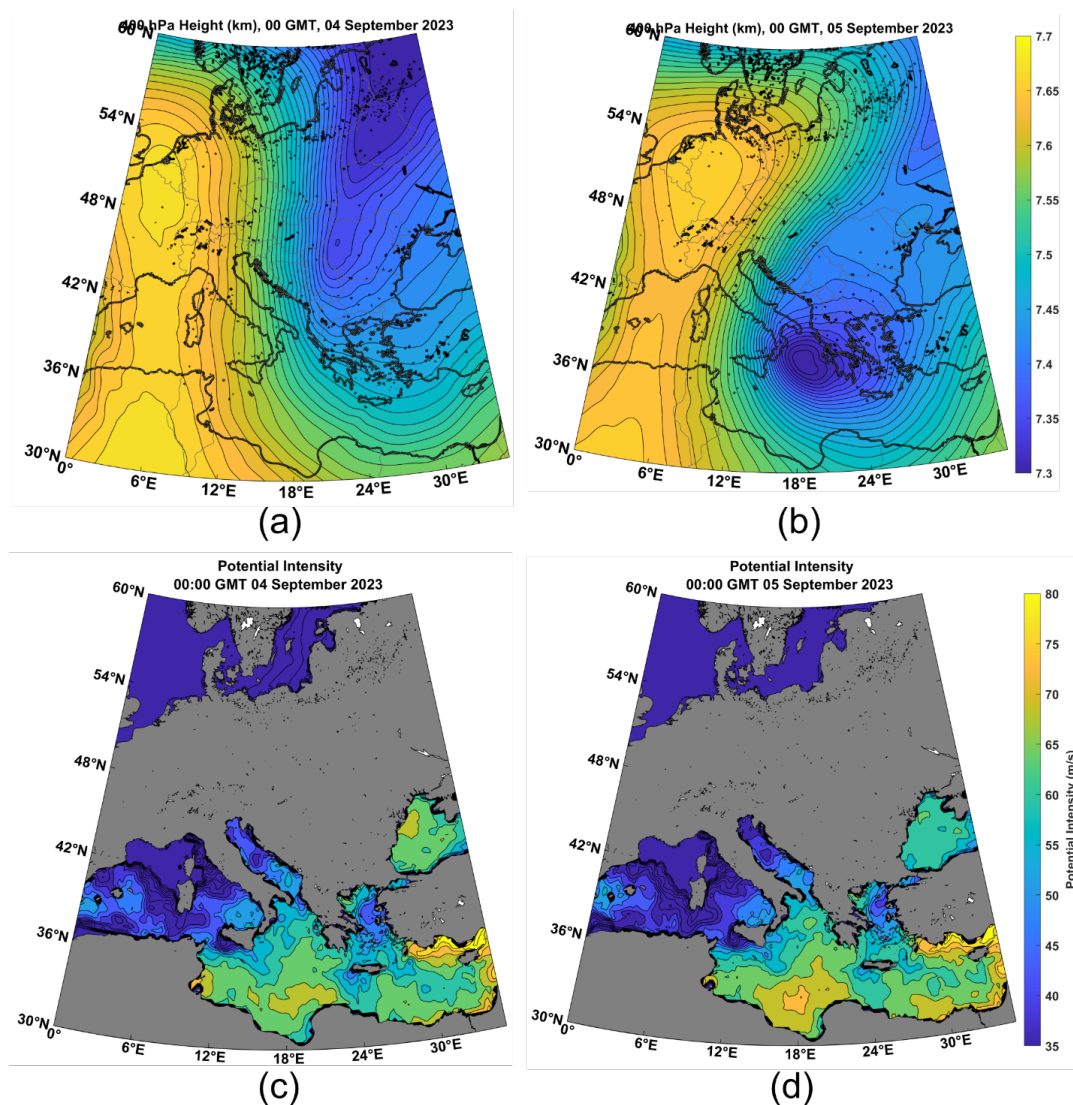


568

569 *Figure 27: NOAA-20 VIIRS image of Storm Daniel at 12 GMT 9 September 2023, as it approached the Libyan coast.*

570

571 As with Zorbas, the antecedent potential intensity was high throughout the Mediterranean south
572 and east of Italy and Sicily, and the event was triggered by a Rossby wave breaking event
573 (Figure 28). And as with Zorbas, the cutoff cyclone aloft was not strong enough to appreciably
574 alter the existing potential intensity but acted as a trigger for the tropical cyclone that Daniel
575 became. This was another classic case of tropical transition, and not a cyclop.



576

577 *Figure 28: 400 hPa geopotential height (km; (a)-(b)) and actual potential intensity (ms⁻¹; (c)-(d)) at 00 GMT*
 578 *September 4th ((a) and (c)) and 5th ((b) and (d)), from ERA-5 reanalyses.*

579 Yet Storm Daniel differed from Zorbas in one important respect: as it approached the Libyan
 580 coast around September 10th, it came under the influence of strong high-level potential vorticity
 581 (PV) advection owing to a mesoscale “satellite” PV mass rotating around the principal upper-
 582 level cutoff cyclone (Figure 29). The quasi-balanced forcing associated with the superposition of
 583 the high-level PV anomaly with the surface-based warm core probably contributed to Daniel’s
 584 intensification which, remarkably for a surface flux-driven cyclone, continued after landfall
 585 (Hewson et al., 2024).

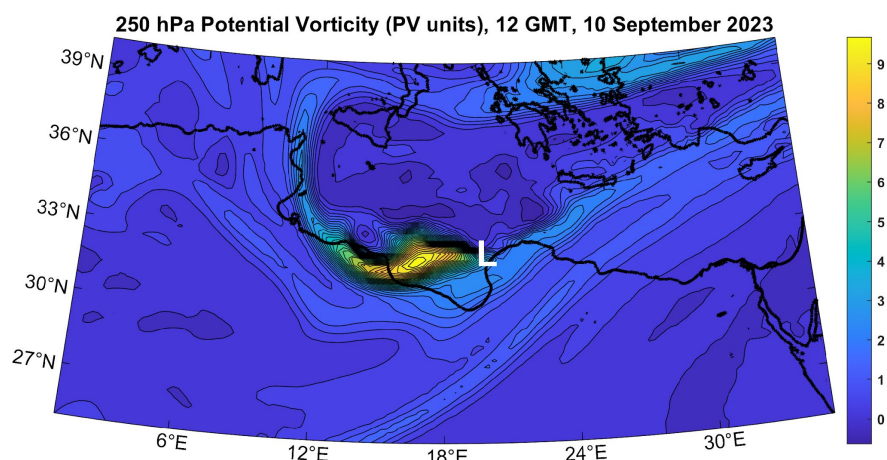


Figure 29: Potential vorticity (PV units, $10^{-6} \text{ K kg}^{-1} \text{ m}^2 \text{ s}^{-1}$) at 250 hPa at 12 GMT on 10 September, 2023. The white "L" marks the approximate surface center of Daniel at this time.

5. Summary and conclusions

We here argue that many of the cyclonic storms called medicanes, polar lows, subtropical cyclones, and Kona storms operate on the same physics and ought to be identified as a single class of storms that we propose to call cyclops. Like classical tropical cyclones, these are driven primarily by wind-dependent surface enthalpy (latent and sensible heat) fluxes, but unlike classical TCs, there is little or no climatological potential intensity for the storms. Rather, the development and approach of strong, cold-core cyclones in the upper troposphere cools and moistens the column through dynamical lifting, generating mesoscale to synoptic scale columns with elevated potential intensity and humidity, and reduced wind shear – ideal embryos for the development of surface flux-driven cyclones.

We do not expect cyclops to last as long as classical TCs. In the first place, the conditions that enable such storms are confined in space and transient in time. For example, the cutoff cyclone aloft is often re-absorbed into the main baroclinic flow. In addition, the strong surface enthalpy fluxes that power cyclops also increase the enthalpy of the otherwise spatially limited cold columns in which they form, reducing over time the thermodynamic disequilibrium between the air column and the sea surface. A back-of-the-envelope estimate for the time to destroy the initial thermodynamic disequilibrium is on the order of days. By contrast, even the strongest classical TCs do not sufficiently warm the large expanses of the tropical troposphere they influence to appreciably diminish the large-scale potential intensity of tropical warm pools.

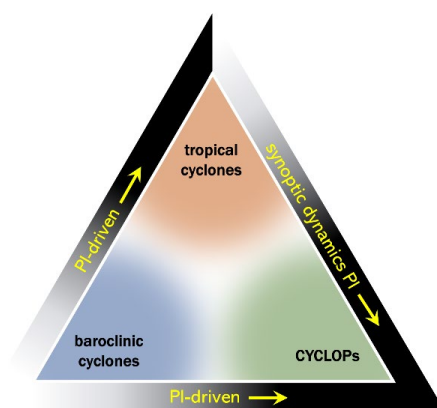
Not all cyclonic storms that have been called polar lows, medicanes, subtropical cyclones, or Kona storms meet our definition of cyclop. The literature describes many polar lows that have



611 been traced to something more nearly like classical baroclinic instability acting in an air mass of
 612 anomalously low static stability (e.g. Sardie and Warner, 1985). Many storms identified as Kona
 613 storms because of their location and season, and which developed under cold cyclones aloft,
 614 never received much of a boost from surface fluxes and therefore would not be classified as
 615 cyclops. And, as we described in the last section, two strong Mediterranean cyclones, Zorbas of
 616 2018 and Daniel of 2023, developed in environments of high climatological potential intensity
 617 and formed via the tropical transition process.

618 Beyond these caveats, not all cold-core, closed cyclones in the upper troposphere that develop
 619 or move over relatively warm ocean waters develop cyclops. Without doing a comprehensive
 620 survey, we have found several cases of greatly enhanced potential intensity under cold lows
 621 aloft that did not develop strong, concentrated surface cyclones. We suspect that, as with
 622 classical tropical cyclones, dry air incursions above the boundary layer may have prevented
 623 genesis in these cases, but as these events generally occur in regions devoid of in-situ
 624 observations, it is not clear how well reanalyses capture variations of moisture on the scale of
 625 cyclops. In any event, the efficiency with which upper-level cut-off cyclones produce cyclops,
 626 given a substantial perturbation in potential intensity, should be a subject of future research.

627 Clearly, there exists a continuum between pure tropical transition, in which synoptic-scale
 628 dynamics play no role in setting up the potential intensity, and pure cyclops in which synoptic-
 629 scale processes create all the potential intensity that drives the storm. We might think of a
 630 triangular phase space in which the vertices are pure baroclinic cyclones, pure tropical
 631 cyclones, and cyclops, with real storms migrating through that phase space over time, as in
 632 phase-space diagrams of (Hart, 2003). This proposed phase space is illustrated in Figure 30.



633

634 *Figure 30: Proposed phase space for baroclinic cyclones, tropical cyclones, and cyclops. AT the lower left corner,*
 635 *pure baroclinic cyclones are driven by ambient baroclinity. At the upper corner, pure tropical cyclones are driven by*
 636 *ambient potential intensity (PI) arising from the thermodynamic disequilibrium between the ocean and atmosphere. At*
 637 *the lower right corner, pure CYCLOPs are driven by PI locally generated by synoptic scale dynamical processes, in*
 638 *the absence of climatological PI. As with Hart's cyclone phase space (Hart, 2003), individual cyclones can migrate*
 639 *through this space over time.*



Synoptic scale processes, like Rossby wave breaking, are essential not only for triggering cyclops but for providing conducive thermodynamic and kinematic environments for their development. As such, forecasters must account for both the triggering potential and mesoscale to synoptic scale environmental development in predicting the formation and evolution of cyclops. The modified potential intensity (V_{pm}) introduced here may prove to be a valuable diagnostic that can easily be calculated from NWP model output. To simulate cyclops, NWP models need to make accurate forecasts of baroclinic processes that lead to the formation and humidification of deep cold pools aloft, and be able to handle surface fluxes and other boundary layer processes essential to the formation of surface flux-driven cyclones. And, as with tropical cyclones, coupling to the ocean is essential for accurate intensity prediction.

Finally, we encourage researchers to focus on the essential physics of cyclops regardless of where in the world they occur. Casting a broader geographical net will harvest a greater sample of such storms and should lead to more rapid progress in understanding and forecasting them.

653

654 Appendix

Potential intensity is a measure of the maximum surface wind speed that can be achieved by a cyclone fueled entirely by surface enthalpy fluxes. It is defined (see Rousseau-Rizzi and Emanuel (2019) for an up-to-date definition):

$$658 \quad V_p^2 = \frac{C_k}{C_D} \frac{T_s - T_o}{T_o} (h_0^* - h_b), \quad (A1)$$

Where C_k and C_D are the surface exchange coefficients for enthalpy and momentum, T_s and T_o are the absolute temperatures of the surface and outflow layer, h_0^* is the saturation moist static energy of the sea surface, and h_b is the moist static energy of the boundary layer.

Using the relation $T\delta s \approx \delta h$, where s is moist entropy, we can re-write (A1) slightly as

$$663 \quad V_p^2 = \frac{C_k}{C_D} \frac{T_s - T_o}{T_o} T_s (s_0^* - s_b). \quad (A2)$$

Next, we assume that the troposphere near cyclops has a nearly moist adiabatic lapse rate, and the moist entropy of the boundary layer is equal to the saturation moist entropy, s^* , of the troposphere; i.e., that the troposphere is neutrally stable to moist adiabatic ascent from the boundary layer. Under these conditions, (A2) may be re-written

$$668 \quad V_p^2 = \frac{C_k}{C_D} \frac{T_s - T_o}{T_o} T_s (s_0^* - s^*). \quad (A3)$$



669 Here s^* is constant with altitude, since the troposphere is assumed to have a moist adiabatic
 670 lapse rate.

671 Referring to Figure 1a in the main text, we want to know what the potential intensity is under the
 672 cutoff cyclone aloft *before* the atmosphere underneath it has started to warm up under the
 673 influence of surface enthalpy fluxes. But in reality, this warming commences as soon as the
 674 system moves over relatively warm water. We can infer what the temperature, or s^* , is under
 675 the cutoff cyclone by relating the temperature perturbation under the cyclone to the geopotential
 676 perturbation associated with the cutoff low.

677 We begin with the perturbation hydrostatic equation in pressure coordinates:

$$678 \quad \frac{\partial \phi'}{\partial p} = -\alpha', \quad (A4)$$

679 where ϕ' is the perturbation geopotential and α' is the perturbation specific volume. Since the
 680 latter is a function of pressure and s^* only, we can use the chain rule and one of the Maxwell
 681 relations from thermodynamics (Emanuel, 1994) to write (A4) as

$$682 \quad \frac{\partial \phi'}{\partial p} = - \left(\frac{\partial T}{\partial p} \right)_{s^*} s^{*'} . \quad (A5)$$

683 Now, since $s^{*'}$ does not vary with altitude, we can integrate (A5) from the surface to the local
 684 tropopause to yield

$$685 \quad \phi_{cl}' - \phi_s' = (T_s - T_o) s^{*'} . \quad (A6)$$

686 where ϕ_{cl}' is the geopotential perturbation associated with the cutoff cyclone aloft and ϕ_s' is the
 687 near-surface geopotential perturbation.

688 We want to know how cold the air is under the cutoff low *before* the surface pressure has
 689 dropped, so we can use (A6) to find the temperature (or s^*) perturbation that would be found
 690 under the cutoff cyclone in the absence of a surface pressure perturbation:

$$691 \quad s^{*'} = \frac{\phi_{cl}'}{T_s - T_o} . \quad (A7)$$

692 Using this, the modified definition of potential intensity, V_{pm} , can be written from (A1) as

$$693 \quad V_{pm}^2 = \frac{C_k}{C_D} \frac{T_s - T_o}{T_o} T_s \left(s_0^* - s_e^* - \frac{\phi_{cl}'}{T_s - T_o} \right), \quad (A8)$$



694 or equivalently,

$$695 \quad V_{pm}^2 = V_p^2 - \frac{C_k}{C_D} \frac{T_s}{T_o} \phi_{cl}, \quad (A9)$$

696 where V_p is the unperturbed potential intensity, and s_e^* is the unperturbed environmental
 697 saturation entropy. We use (A9) in the calculations reported in this paper, with V_p calculated
 698 using the algorithm of Bister and Emanuel (2002).

699 For the purposes of the present work, we defined the perturbation as the difference between the
 700 actual geopotential and its climatological value determined from monthly mean values over the
 701 period 1979-2023, and we estimate the cutoff cyclone geopotential perturbation at 400 hPa.

702 Code and data availability

703 No modeling was performed in the course of this work, and no code developed except to plot
 704 reanalysis data. Routines for calculating potential intensity are available at
 705 <https://github.com/dgilford/tcpypI>. All of the meteorological analyses presented herein are
 706 based in ERA5 downloaded from the Copernicus Climate Change Service
 707 (<https://doi.org/10.24381/cds.143582cf>, Hersbach et al., 2020).

708 Author contributions

709 KE carried out the analyses and prepared the manuscript with contributions from all the co-
 710 authors. JJG prepared Figure 30.

711 Competing interests

712 The authors declare that they have no conflict of interest.

713 Acknowledgements

714 This paper was motivated by discussions at the TROPICANA (TROPIcal Cyclones in
 715 ANthropocene: physics, simulations & Attribution) program, which took place in June 2024 at
 716 the Institute Pascal, University of Paris-Saclay, and aimed to address complex issues related to
 717 tropical cyclones, medicanes, and their connection with climate change.

718 This work was made possible by Institut Pascal at Université Paris-Saclay with the support of
 719 the program TROPICANA, “Investissements d’avenir” ANR-11-IDEX-0003-01.

720 T.Alberti acknowledges useful discussions within the MedCyclones COST Action (CA19109)
 721 and the FutureMed COST Action (CA22162) communities.

722 S. Bourdin received financial support from the NERC-NSF research grant n° NE/W009587/1
 723 (NERC) & AGS-2244917 (NSF) Hurricane Risk Amplification and Changing North Atlantic



724 Natural disasters (Huracan), and from the EUR IPSL-Climate Graduate School through the
 725 ICOCYCLONES2 project, managed by the ANR under the "Investissements d'avenir"
 726 programme with the reference 37 ANR-11-IDEX-0004 - 17-EURE-0006.

727 S.J. Camargo and C.-Y. Lee acknowledge the support of the U.S. National Science Foundation
 728 (AGS 20-43142, 22-17618, 22-44918) and U.S. Department of Energy (DOE) (DE-
 729 SC0023333).

730 K. Emanuel was supported by the U.S. National Science Foundation under grant AGS-2202785.

731 M. M. Miglietta was partly supported by "Earth Observations as a cornerstone to the
 732 understanding and prediction of tropical like cyclone risk in the Mediterranean (MEDICANES)",
 733 ESA Contract No. 4000144111/23/I-KE.

734 H. Ramsay acknowledges funding support from the Climate Systems Hub of the Australian
 735 Government's National Environmental Science Program (NESP).

736 R. Romero acknowledges financial support by the "Ministerio de Ciencia e Innovación" of Spain
 737 through the grant TRAMPAS (PID2020-113036RB-I00/AEI/10.13039/501100011033).

738

739 References

740 Bister, M. and Emanuel, K. A.: Low frequency variability of tropical cyclone potential intensity, 1:
 741 Interannual to interdecadal variability, *J Geophys Res*, 107, doi:10.1029/2001JD000776, 2002.

742 Bosart, L. F. and Bartlo, J. A.: Tropical storm formation in a baroclinic environment, *Mon Wea*
 743 *Rev*, 119, 1979–2013, 1991.

744 Cangliosi, J. P., Papin, P., and Beven, J. L.: Unnamed tropical storm (AL012023)., 2023.

745 Cavicchia, L., von Storch, H., and Gualdi, S.: A long-term climatology of medicanes, *Clim. Dyn.*,
 746 43, 1183–1195, <https://doi.org/10.1007/s00382-013-1893-7>, 2014.

747 Cavicchia, L., Pepler, A., Dowdy, A., and Walsh, K.: A physically based climatology of the
 748 occurrence and intensification of Australian East Coast Lows, *J. Clim.*, 32, 2823–2841,
 749 <https://doi.org/10.1175/JCLI-D-18-0549.1>, 2019.

750 Chavas, D. R. and Emanuel, K. A.: Equilibrium tropical cyclone size in an idealized state of
 751 axisymmetric radiative–convective equilibrium, *J Atmos Sci*, 71, 1663–1680, 2014.

752 Cronin, T. W. and Chavas, D. R.: Dry and semidry tropical cyclones, *J. Atmospheric Sci.*, 76,
 753 2193–2212, <https://doi.org/10.1175/jas-d-18-0357.1>, 2019.

754 Daingerfield, L. H.: Kona storms, *Mon. Weather Rev.*, 49, 327–329,
 755 [https://doi.org/10.1175/1520-0493\(1921\)49<327:ks>2.0.co;2](https://doi.org/10.1175/1520-0493(1921)49<327:ks>2.0.co;2), 1921.



- 756 Davis, C. A. and Bosart, L. F.: Baroclinically induced tropical cyclogenesis, *Mon. Weather Rev.*,
 757 131, 2730–2747, [https://doi.org/10.1175/1520-0493\(2003\)131<2730:BITC>2.0.CO;2](https://doi.org/10.1175/1520-0493(2003)131<2730:BITC>2.0.CO;2), 2003.
- 758 Davis, C. A. and Bosart, L. F.: The TT problem: Forecasting the tropical transition of cyclones,
 759 *Bull. Am. Meteorol. Soc.*, 85, 1657–1662, <https://doi.org/10.1175/BAMS-85-11-1657>, 2004.
- 760 Emanuel, K.: Genesis and maintenance of “Mediterranean hurricanes,” *Adv Geosci*, 2, 217–
 761 220, 2005.
- 762 Emanuel, K.: Tropical cyclone activity downscaled from NOAA-CIRES reanalysis, 1908–1958, *J*
 763 *Adv Model Earth Sys*, 2, 1–12, 2010.
- 764 Emanuel, K. A.: *Atmospheric Convection*, Oxford Univ. Press, New York, 580 pp., 1994.
- 765 Evans, J. L. and Braun, A.: A climatology of subtropical cyclones in the South Atlantic, *J. Clim.*,
 766 25, 7328–7340, <https://doi.org/10.1175/JCLI-D-11-00212.1>, 2012.
- 767 Fita, L. and Flaounas, E.: Medicanes as subtropical cyclones: the December 2005 case from
 768 the perspective of surface pressure tendency diagnostics and atmospheric water budget, *Q. J.*
 769 *R. Meteorol. Soc.*, 144, 1028–1044, <https://doi.org/10.1002/qj.3273>, 2018.
- 770 Flaounas, E., Dafis, S., Davolio, S., Faranda, D., Ferrarin, C., Hartmuth, K., Hochman, A.,
 771 Koutroulis, A., Khodayar, S., Miglietta, M. M., Pantillon, F., Patlakas, P., Sprenger, M., and
 772 Thurnherr, I.: Dynamics, predictability, impacts, and climate change considerations of the
 773 catastrophic Mediterranean Storm Daniel (2023), *EGUsphere*, 2024, 1–29,
 774 <https://doi.org/10.5194/egusphere-2024-2809>, 2024.
- 775 Gozzo, L. F., Rocha, R. P. da, Reboita, M. S., and Sugahara, S.: Subtropical cyclones over the
 776 southwestern South Atlantic: Climatological aspects and case study, *J. Clim.*, 27, 8543–8562,
 777 <https://doi.org/10.1175/JCLI-D-14-00149.1>, 2014.
- 778 Hart, R. E.: A cyclone phase space derived from thermal wind and thermal asymmetry, *Mon.*
 779 *Weather Rev.*, 131, 585–616, [https://doi.org/10.1175/1520-0493\(2003\)131<0585:acpsdf>2.0.co;2](https://doi.org/10.1175/1520-0493(2003)131<0585:acpsdf>2.0.co;2), 2003.
- 781 Hersbach, H., Bell, B., Berrisford, P., Hirahara, S., Horányi, A., Muñoz-Sabater, J., Nicolas, J.,
 782 Peubey, C., Radu, R., Schepers, D., Simmons, A., Soci, C., Abdalla, S., Abellan, X., Balsamo,
 783 G., Bechtold, P., Biavati, G., Bidlot, J., Bonavita, M., De Chiara, G., Dahlgren, P., Dee, D.,
 784 Diamantakis, M., Dragani, R., Flemming, J., Forbes, R., Fuentes, M., Geer, A., Haimberger, L.,
 785 Healy, S., Hogan, R. J., Hólm, E., Janisková, M., Keeley, S., Laloyaux, P., Lopez, P., Lupu, C.,
 786 Radnoti, G., de Rosnay, P., Rozum, I., Vamborg, F., Villaume, S., and Thépaut, J.-N.: The
 787 ERA5 global reanalysis, *Q. J. R. Meteorol. Soc.*, 146, 1999–2049,
 788 <https://doi.org/10.1002/qj.3803>, 2020.
- 789 Hewson, T., Ashoor, A., Bousetta, S., Emanuel, K., Lagouvardos, K., Lavers, D., Magnusson,
 790 L., Pilloso, F., and Zoster, E.: Medicane Daniel: an extraordinary cyclone with devastating
 791 impacts, *ECMWF Newsl.*, 179, 33–47, 2024.



- 792 Holland, G. J., Lynch, A. H., and Leslie, L. M.: Australian east-coast cyclones. Part I: Synoptic
 793 overview and case study, *Mon. Weather Rev.*, 115, 3024–3036, [https://doi.org/10.1175/1520-](https://doi.org/10.1175/1520-0493(1987)115<3024:AECCPI>2.0.CO;2)
 794 0493(1987)115<3024:AECCPI>2.0.CO;2, 1987.
- 795 McIntyre, M. E. and Palmer, T. N.: Breaking planetary waves in the stratosphere, *Nature*, 305,
 796 593–600, <https://doi.org/10.1038/305593a0>, 1983.
- 797 McTaggart-Cowan, R., Deane, G. D., Bosart, L. F., Davis, C. A., and Galarneau, T. J.:
 798 Climatology of tropical cyclogenesis in the North Atlantic (1948–2004), *Mon. Weather Rev.*, 136,
 799 1284–1304, <https://doi.org/10.1175/2007MWR2245.1>, 2008.
- 800 McTaggart-Cowan, R., Galarneau, T. J., Bosart, L. F., Moore, R. W., and Martius, O.: A global
 801 climatology of baroclinically influenced tropical cyclogenesis, *Mon. Weather Rev.*, 141, 1963–
 802 1989, <https://doi.org/10.1175/MWR-D-12-00186.1>, 2013.
- 803 McTaggart-Cowan, R., Davies, E. L., Fairman, J. G., Galarneau, T. J., and Schultz, D. M.:
 804 Revisiting the 26.5°C sea surface temperature threshold for tropical cyclone development, *Bull.*
 805 *Am. Meteorol. Soc.*, 96, 1929–1943, <https://doi.org/10.1175/BAMS-D-13-00254.1>, 2015.
- 806 Miglietta, M. M. and Rotunno, R.: Development mechanisms for Mediterranean tropical-like
 807 cyclones (medicane), *Q. J. R. Meteorol. Soc.*, 145, 1444–1460, <https://doi.org/10.1002/qj.3503>,
 808 2019.
- 809 Nastos, P. T., Karavana Papadimou, K., and Matsangouras, I. T.: Mediterranean tropical-like
 810 cyclones: Impacts and composite daily means and anomalies of synoptic patterns, *High Impact*
 811 *Atmospheric Process. Mediterr.*, 208, 156–166, <https://doi.org/10.1016/j.atmosres.2017.10.023>,
 812 2018.
- 813 Nordeng, T. E. and Rasmussen, E. A. D.: 10. 1034/j. 1600-0870. 1992. 00001. x: A most
 814 beautiful polar low. A case study of a polar low development in the Bear Island region, *Tellus A*,
 815 44, 81–99, 1992.
- 816 Pytharoulis, I., Craig, G. C., and Ballard, S. P.: Study of the Hurricane-like Mediterranean
 817 cyclone of January 1995, *Phys. Chem. Earth Part B Hydrol. Oceans Atmosphere*, 24, 627–632,
 818 [https://doi.org/10.1016/S1464-1909\(99\)00056-8](https://doi.org/10.1016/S1464-1909(99)00056-8), 1999.
- 819 Romero, R. and Emanuel, K. D.: 10. 1002/jgrd. 50475: Medicanes risk in a changing climate, *J*
 820 *Geophys Res*, 118, 2013.
- 821 Rotunno, R. and Emanuel, K. A.: An air-sea interaction theory for tropical cyclones. Part II., *J*
 822 *Atmos Sci*, 44, 542–561, 1987.
- 823 Rousseau-Rizzi, R. and Emanuel, K.: An evaluation of hurricane superintensity in axisymmetric
 824 numerical models, *J. Atmospheric Sci.*, 76, 1697–1708, <https://doi.org/10.1175/jas-d-18-0238.1>,
 825 2019.
- 826 Sardie, J. M. and Warner, T. T. D.: 10. 1111/j. 1600-0870. 1985. tb00444. x: A numerical study
 827 of the development mechanisms of polar lows, *Tellus A*, 37A, 460–477, 1985.



- 828 Simpson, R. H.: Evolution of the Kona storm: A subtropical cyclone, *J. Atmospheric Sci.*, 9, 24–
 829 35, [https://doi.org/10.1175/1520-0469\(1952\)009<0024:EOTKSA>2.0.CO;2](https://doi.org/10.1175/1520-0469(1952)009<0024:EOTKSA>2.0.CO;2), 1952.
- 830 Tomita, H. and Tanaka, R.: Ocean surface warming and cooling responses and feedback
 831 processes associated with polar lows over the Nordic seas, *J. Geophys. Res. Atmospheres*,
 832 129, e2023JD040460, <https://doi.org/10.1029/2023JD040460>, 2024.
- 833 Tous, M. and Romero, R. D.: 10. 1002/joc. 3428: Meteorological environments associated with
 834 medicane development, *Int. J. Climatol.*, 33, 1–14, 2013.
- 835 Velez-Pardo, M. and Cronin, T. W.: Large-scale circulations and dry tropical cyclones in direct
 836 numerical simulations of rotating Rayleigh-Bénard convection, *J. Atmospheric Sci.*,
 837 <https://doi.org/10.1175/JAS-D-23-0018.1>, 2023.
- 838 Yanase, W. and co-authors: Climatology of polar lows over the Sea of Japan using the JRA-55
 839 reanalysis, *J Clim.*, 29, 419–437, 2016.
- 840 Yarovaya, D. A., Efimov, V. V., Shokurov, M. V., Stanichnyi, S. V., and Barabanov, V. S.: A
 841 quasitropical cyclone over the Black Sea: Observations and numerical simulation, *Phys.*
 842 *Oceanogr.*, 18, 154–167, <https://doi.org/10.1007/s11110-008-9018-2>, 2008.
- 843 Zhang, W., Villarini, G., Scoccimarro, E., and Napolitano, F.: Examining the precipitation
 844 associated with medicanes in the high-resolution ERA-5 reanalysis data, *Int. J. Climatol.*, 41,
 845 E126–E132, <https://doi.org/10.1002/joc.6669>, 2021.
- 846 Zhang, Y., Meng, Z., Zhang, F., and Weng, Y.: Predictability of tropical cyclone intensity
 847 evaluated through 5-yr forecasts with a convection-permitting regional-scale model in the
 848 Atlantic basin, *Wea Forecast.*, 29, 1003–1022, 2014.
- 849